J. Fluid Mech. (1997), *vol.* 341, *pp.* 165–194. Printed in the United Kingdom

The effect of surfactants on drop deformation and on the rheology of dilute emulsions in Stokes flow

By XIAOFAN LI † AND C. POZRIKIDIS

Department of Applied Mechanics and Engineering Sciences,
University of California at San Diego, La Jolla, CA 92093-0411, USA

(Received 10 September 1996 and in revised form 8 January 1997)

The effect of an insoluble surfactant on the transient deformation and asymptotic shape of a spherical drop that is subjected to a linear shear or extensional flow at vanishing Reynolds number is studied using a numerical method. The viscosity of the drop is equal to that of the ambient fluid, and the interfacial tension is assumed to depend linearly on the local surfactant concentration. The drop deformation is affected by non-uniformities in the surface tension due to the surfactant molecules convection–diffusion. The numerical procedure combines the boundary-integral method for solving the equations of Stokes flow, and a finite-difference method for solving the unsteady convection–diffusion equation for the surfactant concentration over the evolving interface. The parametric investigations address the effect of the ratio of the vorticity to the rate of strain of the incident flow, the Péclet number expressing the ability of the surfactant to diffuse, the elasticity number expressing the sensitivity of the surface tension to variations in surfactant concentration, and the capillary number expressing the strength of the incident flow. At small and moderate capillary numbers, the effect of a surfactant in a non-axisymmetric flow is found to be similar to that in axisymmetric straining flow studied by previous authors. The accumulation of surfactant molecules at the tips of an elongated drop decreases the surface tension locally and promotes the deformation, whereas the dilution of the surfactant over the main body of the drop increases the surface tension and restrains the deformation. At large capillary numbers, the dilution of the surfactant and the rotational motion associated with the vorticity of the incident flow work synergistically to increase the critical capillary number beyond which the drop exhibits continuous elongation. The numerical results establish the regions of validity of the small-deformation theory developed by previous authors, and illustrate the influence of the surfactant on the flow kinematics and on the rheological properties of a dilute suspension. Surfactants have a stronger effect on the rheology of a suspension than on the deformation of the individual drops.

1. Introduction

The accumulation of molecules of a foreign species at the interface between two fluids alters the local thermodynamic environment and consequently the nature of the macroscopic interfacial boundary conditions for the dynamics and, in certain cases, for the kinematics of a two-fluid flow (e.g. Adamson 1976; Defay & Prigogine 1966;

† Present address: Department of Mathematics, Ohio State University, 231 W. 18th Ave, Columbus, OH 43210, USA.

Evans & Skalak 1980). Regular amphophilic surfactants consisting of a soluble molecular group and an insoluble tail, and more complex surface-active species such as proteins and lipids, render the interfacial stratum capable of supporting both tangential and normal stresses, and thus allow it to behave effectively like a viscoelastic thin shell. Moreover, under extreme conditions, the molecules of a bilayered interfacial stratum may slip over each other, defying the usual requirement of continuity of velocity across the interface between two viscous fluids.

In theoretical analyses of two-fluid flow, the effect of the interfacial layer has been described in terms of a constitutive equation that relates the discontinuity of the hydrodynamic traction across the interface to the mechanical properties of the interface. Physical constants involved include the surface elasticity, the surface viscosity, and the surface moduli of elasticity (e.g. Mavrovouniotis & Brenner 1993). A formalism under the combined auspices of thin-shell theory and non-Newtonian fluid mechanics is appropriate, and its implementation has facilitated both analysis and computation, especially for large interfacial deformations (Barthès-Biesel & Rallison 1981; Pozrikidis 1995).

Following Boussinesq's observation that impurities act to reduce the velocity of a settling viscous drop, the effect of a surfactant has been investigated systematically for a variety of flows. A prevailing assumption has been that the interfacial stress tensor can be described adequately in terms of an isotropic tension that is a function of temperature and local surfactant concentration. More sophisticated constitutive equations have also been used. In these models, the surfactant molecules are assumed to be convected and diffuse over the interface, as well as be absorbed from and desorbed into the continuous phases according to a certain kinetics law. Early studies of the effect of surfactants are reviewed by Levich & Krylov (1969), Clift, Grace, & Weber (1974) and Harper (1982).

In recent years, there has been a resurgence of interest in interfacial flows with surfactants, in a broad range of applications. He, Dagan & Maldarelli (1991) studied the motion of a spherical drop through a circular tube; Borhan & Mao (1992) considered the motion of deformable drops; Park, Maruvada & Yoon (1994) studied the motion of bubbles in the Hele-Shaw cell. In other related studies, Gaver & Grotberg (1990) investigated the flow induced by a localized concentration of an insoluble surfactant on a thin film; Boulton-Stone (1995) investigated the effect of a surfactant on the behaviour of an axisymmetric bubble bursting at a free surface of a nearly inviscid fluid, also incorporating the effects of sorption kinetics and interfacial viscosity; Lu & Apfel (1991) and Tian, Holt & Apfel (1995) investigated the effect of interfacial rheology on the oscillations of an inviscid drop; Bruijn (1989, 1993) reported observations on the influence of a surfactant on tip streaming; and Ji & Setterwall (1994) studied the instability of a film falling down a vertical wall. Other studies concerning drop deformation will be reviewed later in this introduction. This substantial research activity reflects a desire to realistically describe the behaviour of physical systems that have not been cleansed of organic species and other contaminants.

In this work, we study the deformation of a viscous drop suspended in an ambient fluid of infinite expanse, subject to a specified steady flow whose velocity depends linearly on the spatial coordinates, under conditions of Stokes flow. We assume that the interface is populated by an insoluble surfactant, and that the interfacial stress tensor is adequately described by isotropic surface tension. Our goal is to investigate the effects of inhomogeneities in surface tension arising from concentration variations due to the surfactant molecules convection–diffusion. We refrain from enhancing the interfacial constitutive equation with viscous and non-Newtonian terms expressing

viscoelastic tensions, but acknowledge that an elastic behaviour is implicit in the model of variable surface tension. Our ultimate objective is to describe the effect of the surfactant on the physics of the flow and rheology of a non-dilute suspension of liquid drops. The present study of a solitary drop is a first step towards achieving that goal.

The behaviour of a drop with a clean interface has been studied extensively using both theoretical and experimental methods (Rallison 1984; Stone 1994; Kennedy, Pozrikidis & Skalak 1994), but the effect of a surfactant has received only scant attention. Flumerfelt (1980) carried out an asymptotic expansion applicable to nearly spherical drops suspended in a simple shear or purely extensional flow. His work was generalized and extended by Stone & Leal (1990), who proceeded to study *large* deformations and breakup in an axisymmetric extensional flow using a numerical method. In a subsequent numerical study, Milliken *et al.* (1993) addressed the effect of the viscosity ratio of the drop and ambient fluid λ, time-dependent motion, and the significance of a nonlinear equation of state for the surface tension. More recently, Milliken & Leal (1994) studied the effects of surfactant solubility, and Pawar & Stebe (1996) investigated the effect of interfacial saturation and inter-surfactant cohesion, all for axisymmetric deformations.

The results of the aforementioned studies confirmed that the effect of a surfactant is determined by the balance of the competing action of two physical processes: convection of surfactant toward the stagnation points at the tip of a drop, which tends to lower the surface tension and increase the drop deformation; and dilution of the surfactant due to an increase in the surface area caused by the deformation, which tends to increase the surface tension and restrain the deformation of the drop. Milliken *et al.* (1993) found that the effect of the surfactant is most pronounced when λ is small: discontinuities in the tangential component of the interfacial traction retard the interfacial velocity and cause the drop to behave as though it were occupied by a more viscous fluid.

In this work, we extend the aforementioned numerical studies on drop deformation by considering genuinely three-dimensional non-axisymmetric flows, and moderate and large drop deformations. Even though high computational cost forces us to consider situations where the viscosity of the drop is equal to that of the ambient fluid, we are still left with a substantial parametric space which we explore by a systematic numerical experimentation. We examine, in particular, the effects of the type of the incident flow, and of the diffusivity of the surfactant expressed by the Péclet number of the interfacial flow.

One important limitation of our model is the assumed linear relation between surface tension and surfactant concentration. The assumption can be revoked at the expense of an increased parametric space for the numerical investigation. Pawar & Stebe (1996) pointed out that the linear model may lead to important errors in the predicted behaviour, but it is nevertheless a reasonable starting point, and it is applicable to systems that have not been subjected to extensive contamination. The physical limitations of the linear relation will be discussed in § 2.1 in terms of the dimensionless numbers that chracterize the drop deformation.

The numerical procedure combines the boundary-integral method for computing the velocity field and a finite-difference method for solving the convection–diffusion equation for the surfactant concentration over the evolving interface of the deforming drop. The convection–diffusion equation is written and solved in non-orthogonal curvilinear coordinates on a global interfacial structured grid. The implementation of the boundary-integral method is straightforward, but solving the convection–diffusion

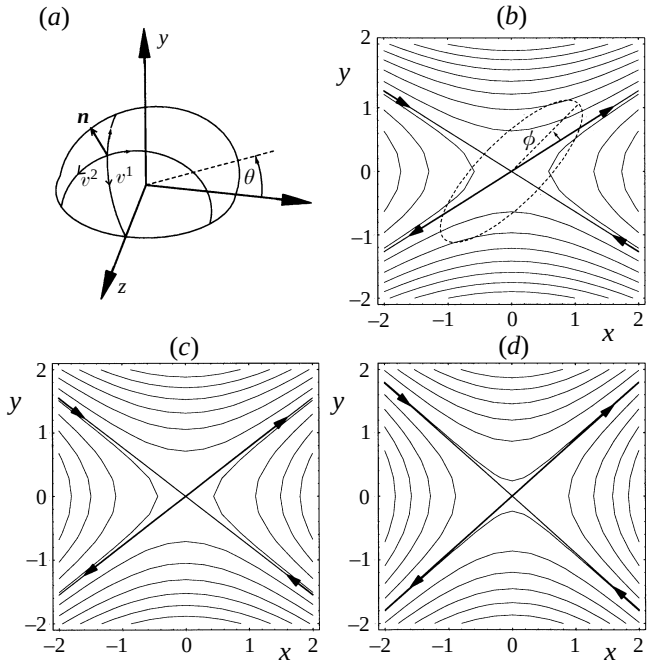

FIGURE 1. (*a*) Schematic illustration of a quarter of a drop deforming under the action of a linear flow. The position of the interface is described in terms of two curvilinear coordinates (v^1, v^2). (*b–d*) Streamlines of the flow field described by equation (2.1) for (*b*) $\chi = 0.4$, (*c*) $\chi = 0.6$, (*d*) $\chi = 0.8$.

equation over the evolving three-dimensional interface requires overcoming important numerical hurdles. In particular, difficulties arise because of the combined action of capillary-type numerical instabilities due to surface tension, and numerical instabilities associated with the integration of the convection–diffusion equation using an explicit numerical method. We overcome these difficulties, at the expense of a substantial computational cost.

2. Problem statement

Consider a neutrally buoyant spherical liquid drop with radius a suspended in an immiscible fluid, as depicted in figure 1(*a*). The viscosity of the drop μ is equal to that of the ambient fluid. The interface is populated with the molecules of an insoluble surfactant whose current and local concentration Γ affects the magnitude of the isotropic interfacial tension in a linear fashion, as will be discussed later in the section. In the undeformed state, the surfactant concentration over the spherical interface has the uniform value Γ_0.

Suddenly, the drop is subjected to a steady incident flow with velocity $\boldsymbol{u}^\infty$ whose components depend linearly on the three spatial coordinates. We restrict our attention to a family of two-dimensional incident flows with velocity

$$\boldsymbol{u}^\infty(\boldsymbol{x}) = \begin{pmatrix} 0 & k & 0 \\ k\chi & 0 & 0 \\ 0 & 0 & 0 \end{pmatrix} \cdot \boldsymbol{x}, \tag{2.1}$$

where the origin has been set at the centre of the drop, k is the shear rate or rate of

extension of the incident flow, and χ is a parameter ranging between 0 and 1; $\chi = 0$ corresponds to simple shear flow, and $\chi = 1$ corresponds to planar extensional flow whose principle axis of stretching forms an angle of 45° with respect to the x-axis. More generally, the ratio between the strength of the vorticity and the rate of strain of the incident flow is given by $\delta = (1-\chi)/(1+\chi)$. The streamline patterns in the (x, y)-plane for $\chi = 0.6$ and 0.8 are shown in figure 1 (c, d).

The orientation of a drop is described by the inclination angle ϕ that is subtended between the largest drop axis and the dividing streamline of the unperturbed flow, as shown in figure 1 (b). For simple shear flow, ϕ is the angle subtended between the longest drop axis and the x-axis.

When the Reynolds number $Re = \rho k a^2/\mu$ is small, where ρ is the density of the drop or the ambient fluid, the motion of the fluid inside and outside the drop is governed by the continuity equation

$$\nabla \cdot \boldsymbol{u} = 0 \tag{2.2}$$

and the Stokes equation

$$-\nabla P + \mu \nabla^2 \boldsymbol{u} = 0, \tag{2.3}$$

where P is the dynamic pressure incorporating the effect of a uniform body force.

The boundary conditions require that the velocity be continuous across the interface, and the interfacial traction vector undergo a discontinuity $\Delta \boldsymbol{f} \equiv (\boldsymbol{\sigma}^{EXT} - \boldsymbol{\sigma}^{INT}) \cdot \boldsymbol{n}$ whose direction and magnitude are determined by the interfacial tension according to the interfacial constitutive equation

$$\Delta \boldsymbol{f} = 2\gamma \kappa_m \boldsymbol{n} - \nabla_s \gamma, \tag{2.4}$$

where γ is the surface tension, κ_m is the mean curvature of the interface, $\boldsymbol{n}$ is the unit vector normal to the interface pointing into the ambient fluid, and $\nabla_s = (\boldsymbol{I} - \boldsymbol{nn}) \cdot \nabla$ is the surface gradient operator acting in the plane that is tangential to the interface.

When the surfactant concentration is small compared to the maximum concentration that corresponds to a saturated interface covered by a monolayer, the equation of state relating the surface tension γ to the surfactant concentration Γ can be linearized to give (Adamson 1976)

$$\gamma_c - \gamma = \Gamma R T, \tag{2.5}$$

where R is the ideal gas constant, T is the absolute temperature, and γ_c denotes the surface tension of the clean interface that is devoid of surfactants. Nonlinear constitutive equations applicable to non-dilute surfactants are discussed by Milliken *et al.* (1993), and Pawar & Stebe (1996).

Assuming further that the surfactant is insoluble in both the drop and the ambient phase, requiring conservation of surfactant molecules over a material interfacial patch (see the Appendix), and stipulating that the interfacial grid lines move with the normal component of the interfacial velocity but do not execute a tangential motion, we find that the evolution of the surfactant concentration Γ is governed by the unsteady convection–diffusion equation

$$\frac{\partial \Gamma}{\partial t} + \nabla_s \cdot (\Gamma \boldsymbol{u}_s - \mathscr{D}_s \nabla_s \Gamma) + 2\Gamma \kappa_m (\boldsymbol{u} \cdot \boldsymbol{n}) = 0, \tag{2.6}$$

where $\partial/\partial t$ denotes the time derivative taken by keeping the values of two curvilinear coordinates defined on the moving interface constant, as will be discussed in § 3 (Stone 1990; Wong, Rumschitzki & Maldarelli 1996); $\boldsymbol{u}_s$ is the component of the fluid velocity vector tangential to the interface, and $\mathscr{D}_s$ is the diffusivity. With

reference to equation (A 9), we have set $\boldsymbol{w} = 0$. The fourth term in equation (2.6) accounts for the effects of stretching of the interface due to normal motion.

To study the effect of surfactant on the transient motion, we solve the coupled system of equations (2.2), (2.3) and (2.6) for the interfacial velocity and surfactant concentration. On one hand, the interfacial velocity depends on the surfactant concentration through the boundary condition (2.4) and equation of state (2.5). On the other hand, computing the rate of change of the surfactant concentration requires a knowledge of the interfacial velocity field as shown in equation (2.6). The coupling necessitates a unified numerical approach.

2.1. *Dimensionless parameters*

Non-dimensionalizing all variables using the undeformed drop radius a as characteristic length, ka as characteristic velocity, and μk as characteristic stress, we find that the deformation of the drop depends on the following dimensionless parameters:

(a) the Péclet number $Pe = ka^2/\mathscr{D}_s$, expressing the relative importance of surfactant convection and diffusion in the plane of the interface;

(b) the elasticity parameter $\beta = \Gamma_0 RT/\gamma_c$, expressing the sensitivity of surface tension to variations in surfactant concentration; from equation (2.5), the initial equilibrium value of surface tension γ_0 is given by $\gamma_0 = \gamma_c(1-\beta)$;

(c) the capillary number $Ca = \mu ka/\gamma_0$, expressing the ratio between the magnitude of viscous stresses due to the incident shear flow, and that of surface tension. The reduction in surface tension from γ_c to γ_0 is built into the definition of capillary number Ca.

In order to study the effect of shear rate or rate of extension k on the deformation of a drop keeping all other parameters constant, we introduce the property number $\alpha = Pe/Ca = a\gamma_0/\mathscr{D}_s\mu$.

In summary, the deformation of the drop is a function of the four dimensionless parameters χ or δ, β, Pe, and Ca. One of the last two parameters Pe and Ca can be replaced with the property number α. In our numerical studies, we consider values in the ranges: $0 \leqslant \chi \leqslant 0.8, 0 \leqslant Pe \leqslant 400, 0 \leqslant \beta \leqslant 0.8, 0 \leqslant Ca \leqslant 1$.

It is important to note that since a linearized equation of state (2.5) has been assumed for the surface tension, the elasticity parameter β is inherently restricted to small values, i.e. $\beta \ll 1$. Thus, the change in the surface tension due to the surfactant must be small relative to the value of surface tension corresponding to a clean interface. Consequently, the computational results for $\beta \geqslant 0.5$ may not be physically meaningful, though they are still interesting from a mathematical standpoint.

2.2. *Summary of results for $Pe = 0$ or $\beta = 0$ (uniform surface tension)*

As a point of reference for our numerical results, we briefly review the behaviour of a drop with constant surface tension placed in a linear shear flow (Rallison 1984; Stone 1994). This behaviour is relevant to the asymptotic limits $\beta \to 0$ or $Pe \to 0$ corresponding, respectively, to situations where the surface tension is insensitive to the surfactant concentration, or else surfactant gradients are smeared out by the dominant action of diffusion, where allowance has been made for the surfactant dilution.

Previous studies have shown that, as the value of the capillary number is increased from zero, an initially spherical drop becomes increasingly more elongated for any value of the viscosity ratio λ. In certain cases, there is a critical value of the capillary number Ca_{cr}, beyond which the drop is not capable of maintaining a steady shape: it stretches, and eventually disintegrates. The value of Ca_{cr} depends on the strength of

the rotational component relative to that of the straining component of the incident flow δ, and on the viscosity ratio λ.

When $\lambda \gg 1$ and the vorticity of the imposed flow is sufficiently strong, the drop maintains a nearly spherical shape even when $Ca \gg 1$; when λ is on the order of unity and $0.2 \leqslant \chi \leqslant 1$, the drop continues to deform and finally disintegrates when $Ca \gg 1$; when $\lambda \ll 1$ and $0.2 \leqslant \chi \leqslant 1$, breakup occurs at higher values of Ca compared to that for drops with λ on the order of unity. In particular, for simple shear flow, $\chi = 0$, the critical capillary number is an increasing function of λ when $\lambda \geqslant 1$, and a decreasing function of λ for $\chi \geqslant 0.6$ and $1 \leqslant \lambda \leqslant 5$.

When $\lambda \ll 1$, the most elongated steady drop shape is long and slender; when $\lambda > 0.1$, it is roughly ellipsoidal; and when $\lambda \gg 1$, it is close to a sphere.

2.3. *Small-deformation theory*

When the drop deformation is small and the surfactant concentration is nearly uniform ($Pe \ll 1$), the leading-order solution for the time-dependent problem governed by equations (2.1)–(2.6) gives (Stone & Leal 1990)

$$D = \frac{5}{8}\frac{35+4\epsilon}{20+2\epsilon}(1+\chi)Ca, \quad \frac{\Gamma}{\Gamma_0} = 1 + \frac{5\alpha Ca}{20+2\epsilon}\frac{\boldsymbol{x}\cdot\boldsymbol{E}\cdot\boldsymbol{x}}{r^2}, \tag{2.7}$$

where D and ϵ are defined as

$$D = (A-B)/(A+B), \quad \epsilon = \beta\alpha/(1-\beta). \tag{2.8}$$

$2A$ and $2B$ are respectively the largest and smallest drop dimension, and $\boldsymbol{E}$ is the rate-of-strain tensor of the incident flow. Thus, the drop deformation increases as the magnitude of ϵ is raised; at a fixed dimensionless shear rate Ca this occurs by increasing α or β. Inspection of the magnitudes of the numerical coefficients in equation (2.7) shows that the effect of the surfactant on the drop deformation parameter D is rather small.

3. Numerical method

We describe the interface in a parametric manner, in terms of two curvilinear coordinates v^1 and v^2, and with reference to an evolving interfacial grid. At the initial instant, the grid lines are spaced evenly with respect to arclength in their respective directions, as shown in figure 1 (*a*). Variables expressing geometrical and physical properties of the interface, including the normal vector $\boldsymbol{n}$ and surfactant concentration Γ, are assigned values at the intersections of the grid lines, $\boldsymbol{x}_{mn}$. The partial derivatives of these variables with respect to surface coordinates v^1 and v^2 are computed using the five-point differentiation formula (e.g. Abramowitz & Stegun 1972, Chap. 25).

3.1. *Boundary-integral formulation*

Following the standard boundary-integral formulation of Stokes flow, we obtain an integral representation for the velocity at a point $\boldsymbol{x}_0$ that is located inside the drop, outside the drop, or at the interface S_D, in terms of the incident velocity $\boldsymbol{u}^\infty$ and a single-layer potential due to the discontinuity in the traction across the interface $\Delta\boldsymbol{f}$ given in equation (2.4),

$$u_j(\boldsymbol{x}_0) = u_j^\infty(\boldsymbol{x}_0) - \frac{1}{8\pi\mu}\int_{S_D} \Delta f_i(\boldsymbol{x}) S_{ij}(\boldsymbol{x},\boldsymbol{x}_0)\,\mathrm{d}S(\boldsymbol{x}), \tag{3.1}$$

where the kernel $\boldsymbol{S}$ is the three-dimensional free-space Stokeslet (e.g. Pozrikidis 1992). The single-layer integral in (3.1) is approximated with the sum of integrals over planar triangles subtended between three neighbouring marker points. The components of $\Delta \boldsymbol{f}$ and $\boldsymbol{S}$ are assumed to vary in a bi-linear manner over each triangle.

The assumption of equal viscosities has allowed us to obtain an integration representation (3.1) instead of a Fredholm integral equation of the second kind for the interfacial velocity, which would have been the case if the viscosity ratio had any value between zero and infinity except the value of unity.

We describe the evolution of the interface by advancing the position of the grid points with the component of the velocity of fluid normal to the interface,

$$\frac{\mathrm{d}\boldsymbol{x}_{mn}}{\mathrm{d}t} = (\boldsymbol{u}(\boldsymbol{x}_{mn}) \cdot \boldsymbol{n}(\boldsymbol{x}_{mn}))\, \boldsymbol{n}(\boldsymbol{x}_{mn}), \tag{3.2}$$

where $\boldsymbol{u}$ is obtained from equation (3.1).

As the drop elongates, regriding and mesh refinement are applied in order to maintain acceptable accuracy and spatial resolution. A discussion of the technical issues involved in regriding is presented by Li & Pozrikidis (1996). The only new feature is that the surfactant concentration at the new grid lines is also computed by cubic spline interpolation. Distributions of the grid lines after a drop has reached a steady state are shown in figures 3–5 (parts *a*).

3.2. *Evolution of surfactant concentration in curvilinear coordinates*

To evaluate the traction jump $\Delta \boldsymbol{f}(\boldsymbol{x}_s, t)$, we require the surfactant concentration distribution $\Gamma(\boldsymbol{x}_s, t)$. This is obtained by solving the counterpart of the evolution equation (2.6) in surface coordinates (v^1, v^2),

$$\frac{\partial \Gamma}{\partial t} = -\frac{1}{\bar{a}^{1/2}} \frac{\partial}{\partial v^{\xi}} \left[\bar{a}^{1/2} \left(\Gamma u^{\xi} - \mathscr{D}_s a^{\xi\eta} \frac{\partial \Gamma}{\partial v^{\eta}} \right) \right] - 2\Gamma \kappa_m (\boldsymbol{u} \cdot \boldsymbol{n}), \tag{3.3}$$

where

$$\boldsymbol{u}_s = u^{\xi} \boldsymbol{a}_{\xi}, \quad \boldsymbol{a}_{\xi} = \frac{\partial \boldsymbol{x}_s}{\partial v^{\xi}} \quad (\xi = 1, 2), \tag{3.4}$$

and $a^{\xi\eta}$ and $\bar{a}$ are the surface covariant components and determinant of the surface metric tensor (Stone & Leal 1990). The summation convention of repeated indices is implied in equations (3.3) and (3.4).

3.3. *Time-advancing schemes*

The motion of the grid points $\boldsymbol{x}_s$ and the evolution of the surfactant distribution Γ are computed as follows: at the time level t, we evaluate $\Delta \boldsymbol{f}$ from (2.4) and (2.5), and compute the interfacial velocity from the boundary integral equation (3.1); using the computed velocity, we update $(\boldsymbol{x}_s, \Gamma)$ to time $t + \Delta t$ according to (3.2) and (3.3). The particular time-marching scheme is selected according to the magnitude of the Péclet number Pe.

In order to ensure numerical stability, at small Péclet numbers ($Pe < 1$), we use the implicit backward Euler method to advance the solution of the convection–diffusion equation (3.3), and the forward Euler method to advance the position of the marker points. In solving for $\Gamma(t + \Delta t)$, we approximate the velocity field $\boldsymbol{u}(t + \Delta t)$ at time $t + \Delta t$ with that at the beginning of the time step, $\boldsymbol{u}(t)$. Since the time-step size is small, typically on the order of $O(10^{-4}/k)$, the variation of the velocity over the period of a time step is negligibly small. Jacobi's iterative method is used for solving the pertinent system of linear algebraic equations for $\Gamma(t + \Delta t)$ in (3.3). Four to twelve iterations

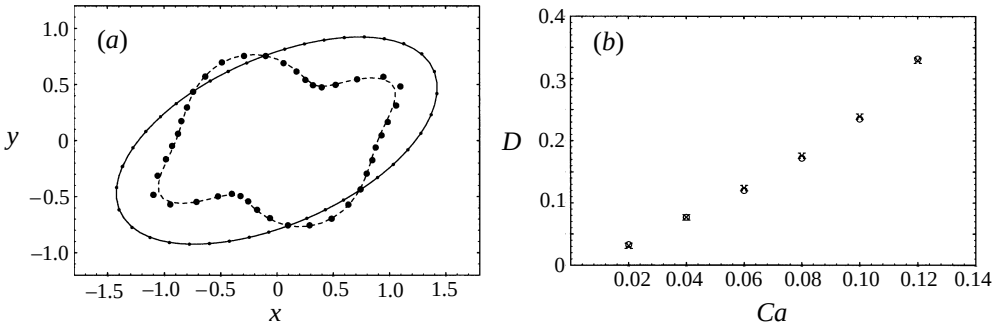

FIGURE 2. (*a*) Convergence of the numerical results with respect to the grid size for $\chi = 0, \alpha = 1000, \beta = 0.3, Ca = 0.3$. The small and large dots represent, respectively, the cross-section of the drop in the (x, y)-plane at the steady state, and associated surfactant concentration, for a coarse 20×10 grid; the solid and dashed lines represent the corresponding quantities for a finer 38×18 grid. (*b*) Testing of the numerical results (x) against those of Stone & Leal (1990) (o) for axisymmetric deformation with $\alpha = 10$ and $\beta = 0.5$. The Taylor drop deformation parameter D is plotted as a function of Ca.

are necessary for the maximum difference between two iterations to become less than 10^{-8} times the converged value. The computational cost of the iterations is negligible compared to that for evaluating the interfacial velocity.

At moderate and large values of Pe, we use the explicit second-order Runge–Kutta method to advance both the position of marker points and the surfactant concentration. For an initial 16×8 grid over a quarter of the drop, the dimensionless time-step size $k\Delta t$ varies from 0.0001 to 0.005, depending on the magnitude of Pe.

The cumulative changes in drop volume and total amount of surfactant were less than 0.5% and 0.1%, respectively, after one thousand time steps. To prevent significant accumulation, at that point we rescale the drop volume and total amount of surfactant to bring them up to their initial values. Similar corrections have been used by previous researchers in cases of axisymmetric motion.

3.4. *Accuracy and validation*

To assess the accuracy of the computations, we compare numerical results for $\chi = 0, \alpha = 1000, \beta = 0.3, Ca = 0.3$, starting with an initial coarse 16×8 grid, and a finer 32×16 grid over a quarter the interface. In figure 2(*a*), we indicate with dots, and plot with solid line, the cross-sections of the drop in the (x, y)-plane at the steady state, and obtain visually indistinguishable shapes. Note that the grid dimensions have increased respectively to 20×10 and 38×18 because of mesh refinement. Figure 2(*a*) also shows the corresponding surfactant concentrations in the (x, y)-plane, plotted with large dots and a dashed line, as polar functions of the meridional angle θ. The radial distance from the origin r is proportional to the surfactant concentration. The results obtained from the coarse and fine grids show small differences, on the order of the numerical error.

The numerical method was also tested by computing the drop deformation in an axisymmetric extensional flow with velocity $\boldsymbol{u}^{\infty} = (kx, -\frac{1}{2}ky, -\frac{1}{2}kz)$, and comparing the results with those of Stone & Leal (1990). These authors used essentially the same numerical method, but with some additional analytical preprocessing that takes advantage of the independence of the flow variables on the azimuthal angle around the drop axis. In this manner, the velocity is computed in terms of a line integral along half the drop contour in the (x, y)-plane, and the convection–diffusion equation

is solved over that line. In figure 2(*b*), we plot the drop deformation parameter D defined in the first of equations (2.8) as a function of Ca, for $\alpha = 10, \beta = 0.5$. The results are nearly indistinguishable within plotting resolution. Additional tests showed excellent agreement.

3.5. *Computational cost*

In the actual implementation of the numerical method, we take advantage of the fore-and-aft symmetry of the interface with respect to the (x, y)-plane, as well as of the point-symmetry with respect to the centre of the drop, and reduce the computational domain to a quarter the surface of the drop. The majority of the computations were performed with an initial 16×8 grid. The steady drop shape and distribution of surfactant at a particular value of the capillary number were used as initial states for a larger value of the capillary number. We assume that steady state has been reached when the maximum norms of both the dimensionless normal velocity $\|\boldsymbol{u}\cdot\boldsymbol{n}\|_\infty$ and the time derivative of surfactant concentration $\|\partial\Gamma/\partial t\|_\infty$ have become less than 0.01.

Depending on the size of the grid, each time step requires 4–200 s of CPU time on a 50MHz SUN SparcStation 20. The number of time steps increases substantially as the capillary number becomes close to the critical value for continued elongation, requiring about 7 days of CPU time on the SparcStation 20 for a complete computation in an extreme case. This high computational cost is the main reason for restricting our attention to instances where the viscosity of the drop is equal to that of the ambient fluid. In spite of laborious efforts, we could not devise a more economical numerical method without compromising accuracy or jeopardizing numerical stability.

4. Results and discussion

We begin by presenting numerical results for three selected combinations of values of χ, α and β; the values of α and β are identical to those considered by Stone & Leal (1990) in their studies of drop deformation in axisymmetric extensional flow. We then proceed to examine the individual effects of the dimensionless parameters β, α and χ.

4.1. *Small Péclet number*

When Pe is small, the dominant process of diffusion keeps the surfactant concentration nearly uniform and the surface tension gradient small throughout the transient deformation. Insolubility requires that the surfactant be diluted by a constant factor that is proportional to the total interfacial area, which increases monotonically in time owing to the interfacial deformation; given the drop volume, the spherical shape has the minimum surface area. In turn, the uniform dilution causes a nearly uniform increase in the surface tension above the initial value. As a consequence, the drop deforms less than a drop whose surface tension is constant, equal to the value at the undeformed state. The latter is hereafter referred to as a *constant surface tension drop.*

Figure 3(*a, b*) shows the steady drop shape, the distribution of surface coordinate lines, and associated surfactant distribution for $\chi = 0.8, \alpha = 0.1, \beta = 0.5$ at $Ca = 0.15$, which corresponds to $Pe = 0.015$. The streamlines of the unperturbed flow are shown in figure 1(*d*). Maximum surfactant concentration or minimum surface tension occurs at the two tips of the interface in the (x, y)-plane; minimum surfactant concentration or maximum surface tension occurs at the waist. The average value of the dimensionless surfactant concentration Γ is approximately 0.9 times the initial

value, whereas its variation over the interface is less than 0.008 the initial value. As predicted by the small-deformation analysis, the fluctuation is on the order of Pe.

To compare the numerical results with the predictions of the small-deformation theory, in figure 3 (c) we plot the surfactant concentration in the (x, y)-plane as a function of the meridional angle θ, for several values of the capillary numbers. The dashed lines show the predictions of the equations (2.7), shifted such that the average value of the concentration is equal to $\overline{\Gamma} = (1/A_D) \int_{S_D} \Gamma(\boldsymbol{x})\, \mathrm{d}S(\boldsymbol{x})$, where A_D is the total area of the interface. The leading-order analysis (2.7) predicts that the average value of the surfactant concentration remains fixed at the initial value Γ_0. Figure 3 (c) shows that, without the shifting, we would have obtained good agreement regarding the shape and magnitude of the fluctuations, but poor agreement regarding the mean value.

The shifting is motivated by our desire to extend the range of validity of the small-deformation theory, and thus make it more useful in engineering practice. The agreement between the solid and dashed lines in figure 3 (c) suggests that higher-order corrections are important with respect to the shifting, but make small contributions to the fluctuations, almost throughout the entire range of capillary numbers where steady shapes are established.

Surfactant conservation requires that $A_D\overline{\Gamma} = 4\pi a^2\Gamma_0$, which provides us with an equation for computing $\overline{\Gamma}$ in terms of A_D. In figure 3 (d), we plot with a solid line A_D at steady state, as a function of the capillary number. The dashed line shows the predictions of the first-order small-deformation theory. Both curves show the expected parabolic behaviour at the origin. The small-deformation theory overestimates the surface area at small and moderate capillary numbers, and underestimates it at larger values of the capillary number. Thus, the first-order theory combined with the insolubility condition would not give accurate estimates of the mean value of the surfactant concentration.

In figure 3 (e), we plot with solid line the deformation parameter D of stationary deformed shapes as a function of capillary number Ca. The dashed line is obtained from the linear prediction (2.7); the dash-dotted line shows the corresponding result for a constant-surface-tension drop. The slopes of the three curves are virtually identical at the origin, and the agreement remains good up to moderate and large deformations, roughly for values of D as high as 0.20. We find that the critical capillary number Ca_{cr} for drop breakup is between 0.15 and 0.16, which is 10% larger than that for a drop with constant surface tension; the latter is about 0.14. In this case, when the capillary number is within the range where steady drops can develop, the Péclet number $Pe = \alpha Ca$ remains less than 0.015. In agreement with Stone & Leal (1990), we find that the surfactant acts to reduce the drop deformation. The corresponding result for the inclination angle ϕ, defined in figure 1 (b), is shown in figure 3 (f). The effect of the surfactant becomes important when the deformation parameter D exceeds the value of 0.20.

Since the fluctuations of the surfactant concentration are small, one should expect that the solid and dashed-dot lines in figure 3 (e,f) will coincide if the capillary number is redefined with respect to the average value of the surface tension corresponding to the stationary deformed shape. To confirm this behaviour, we introduce the corrected capillary number $\overline{Ca} = \mu k a/\overline{\gamma}$, where $\overline{\gamma} = (1/A_D) \int_{S_D} \gamma(\boldsymbol{x})\, \mathrm{d}S(\boldsymbol{x})$. Furthermore, we express $\overline{\gamma}$ in terms of the drop area, by rewriting the linear constitutive equation (2.5) in the equivalent form

$$\gamma(\boldsymbol{x}) = \gamma_0(1 - \beta\Gamma(\boldsymbol{x})/\Gamma_0)/(1 - \beta). \tag{4.1}$$

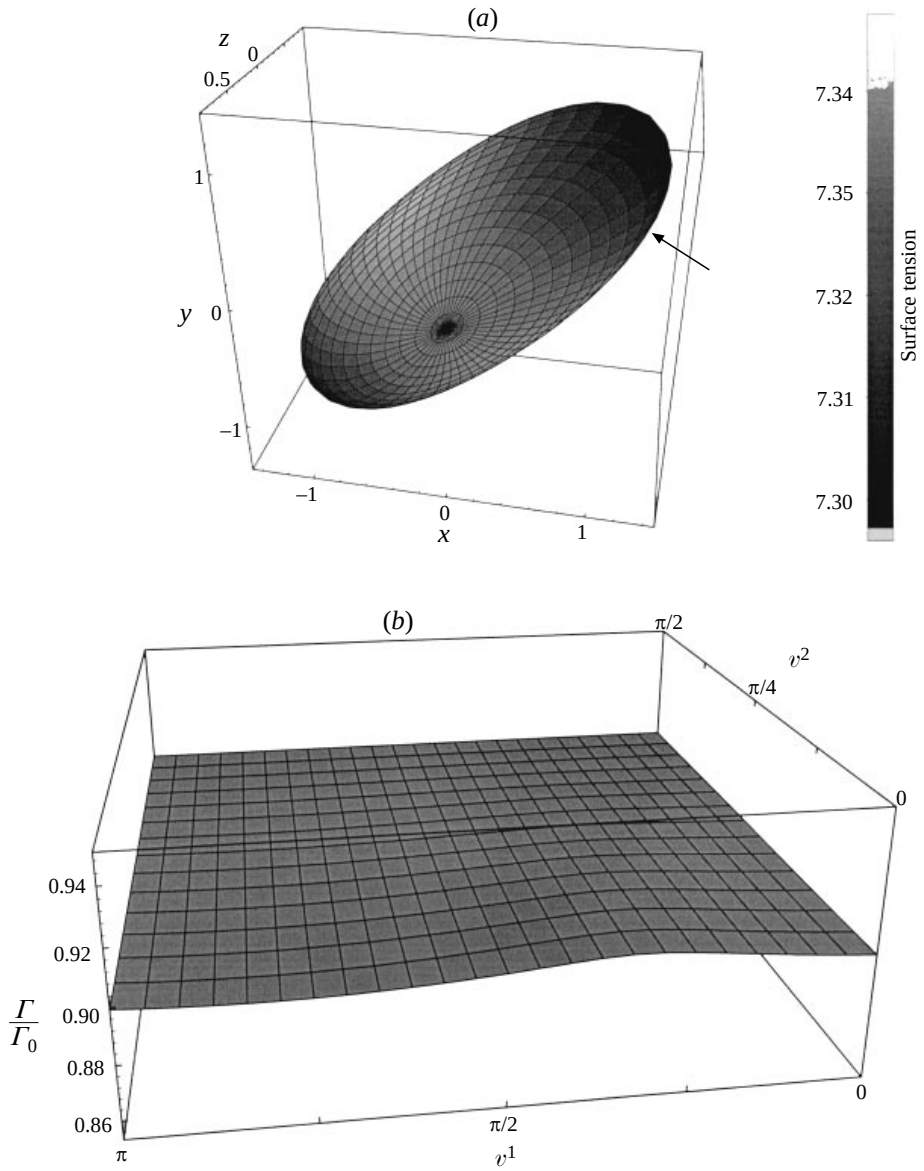

FIGURE 3(*a*, *b*). For caption see facing page.

Integrating (4.1) over the drop surface S_D, and requiring surfactant conservation, we obtain

$$\overline{\gamma} = \gamma_0 \left(1 - \beta 4\pi a^2 / A_D\right) / (1 - \beta), \tag{4.2}$$

which gives

$$\overline{Ca} = Ca(1 - \beta)/(1 - \beta 4\pi a^2 / A_D). \tag{4.3}$$

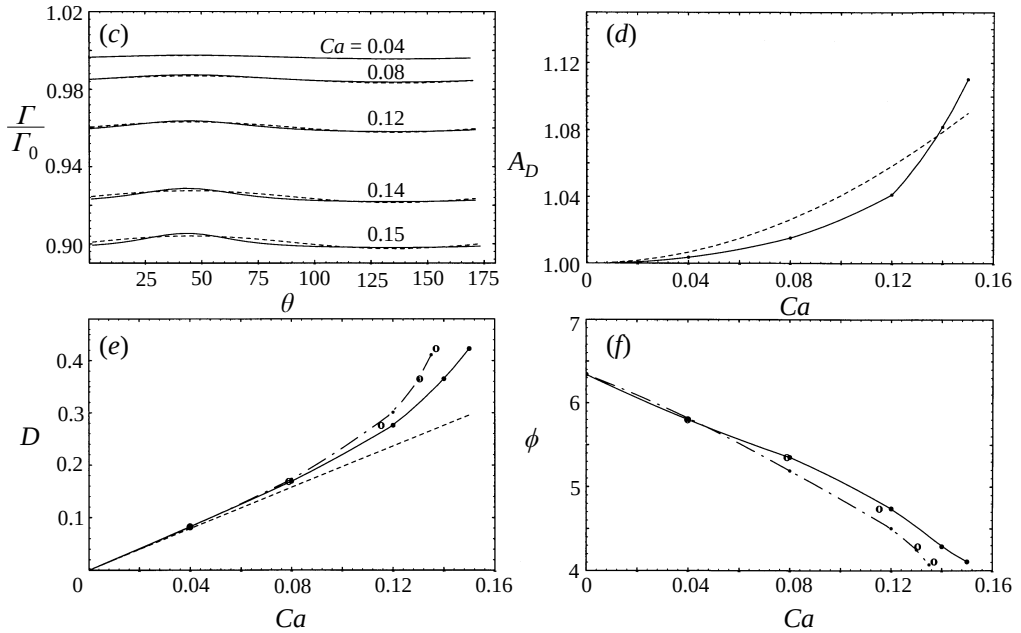

FIGURE 3. Results for a small-Pélect-number case with $\chi = 0.8, \alpha = 0.1, \beta = 0.5$. (*a*) The steady drop shape at $Ca = 0.15$. The shades encode the magnitude of the dimensionless surface tension $\gamma/(\mu k a) = (\gamma/\gamma_0)(1/Ca)$, as shown on the right. (*b*) The corresponding surfactant distribution plotted with respect to the surface curvilinear coordinates. The singular point of the coordinate system corresponds to $v^2 = \pi/2$; the grid point $(v^1, v^2) = (0, 0)$ is shown in (*a*) with an arrow. (*c*) Distribution of the surfactant concentration in the (x, y)-plane for $Ca = 0.04, 0.08, 0.12, 0.14$ and 0.15, plotted as function of the meridional angle θ. (*d*) The drop surface area A_D as function of Ca: ——, numerical simulation; – – –, from the small-deformation theory (2.7). (*e*) The deformation parameter D as function of Ca: ——, for drops with non-uniform surface tension; – – –, from the small-deformation theory (2.7); — - —, for constant-surface-tension drops. (*f*) Same as (*d*), but for the inclination angle ϕ.

In figure 3 (*e,f*), we plot with circles the drop deformation and inclination angle as functions of the corrected capillary number $\overline{Ca}$. The symbols follow closely the curve for constant-surface-tension drops. Thus, given the interfacial area of steady deformed drops with uniform surface tension, we can obtain reasonable estimates for the deformation and inclination of drops with non-uniform surface tension by dividing the capillary number by the factor $(1-\beta 4\pi a^2/A_D)/(1-\beta)$. Extensive numerical results on the deformation of drops with constant surface tensions in simple shear flow have been presented by Kennedy *et al.* (1994), for a wide range of ratios of drop to ambient fluid viscosity.

4.2. $Pe = O(1)$

In the second case study, we consider the deformation of a drop that is immersed in a simple shear flow corresponding to $\chi = 0$, with $\alpha = 10$ and $\beta = 0.1$. These values yield a Péclet number that is on the order of unity. The values of the parameters were chosen so that convective surfactant transport is as important as diffusion. However, because β is small, large surfactant gradients do not cause large variations in surface tension. Consequently, we expect that the drop will behave similarly to a constant-surface-tension drop, at least for small and moderate deformations. This behaviour does indeed emerge from our computations. We find that there is a critical capillary

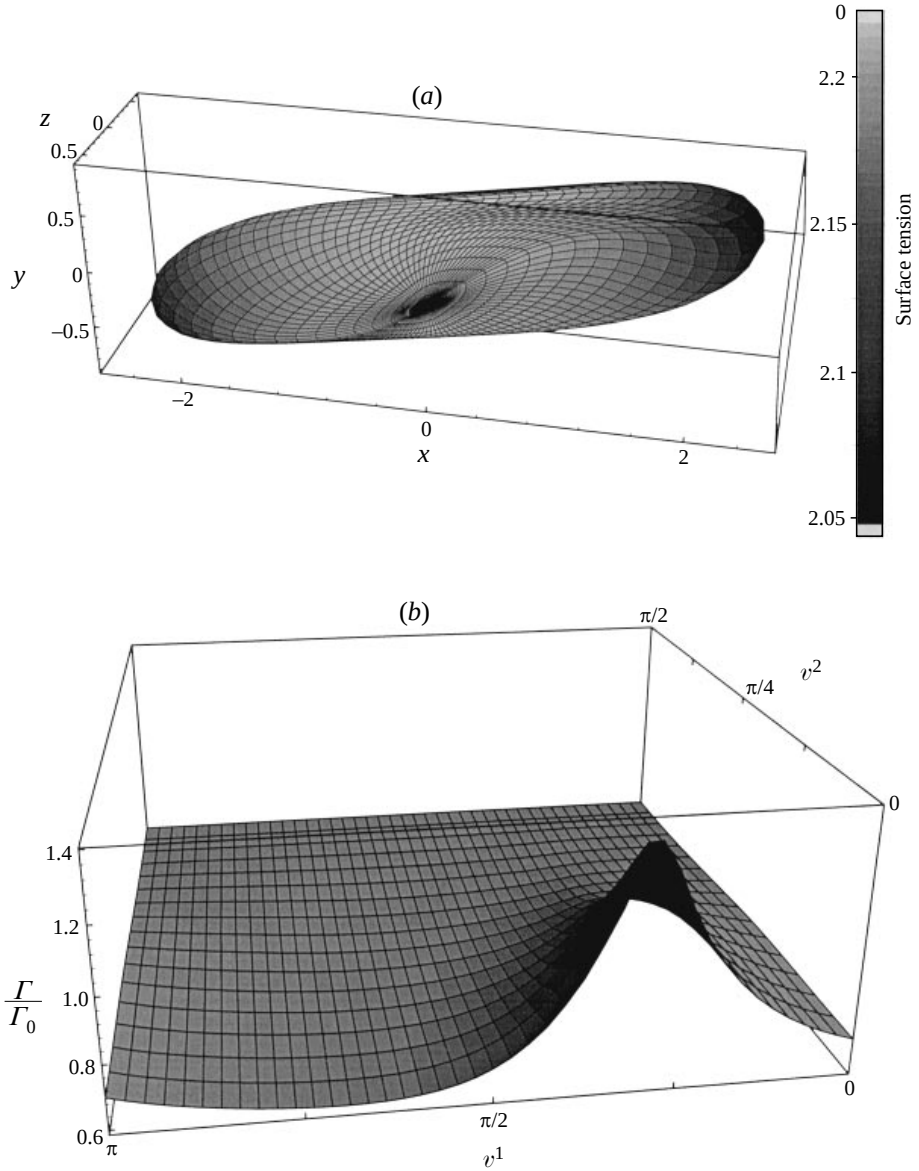

FIGURE 4(*a, b*). For caption see facing page.

number above which the drop continues to elongate under the deforming action of the shear flow. This critical value Ca_{cr} is between 0.47 and 0.48, which is significantly higher than the value 0.44 corresponding to a drop with constant surface tension.

In figure 4 (*a, b*), we display the steady drop shape and associated distribution of the surfactant for $Ca = 0.47$. For higher values of the capillary number, we obtain continuous elongation. The magnitude of the surface tension is coded by the shades shown on the right column. We observe that the drop obtains a cigar-like shape, with a nearly uniform surface tension over the main body, and high-curvature caps at the tips with low surface tension. Although the variation in surfactant concentration exceeds $0.72\Gamma_0$, the variation in surface tension is only $0.08\gamma_0$. It is then not surprising that

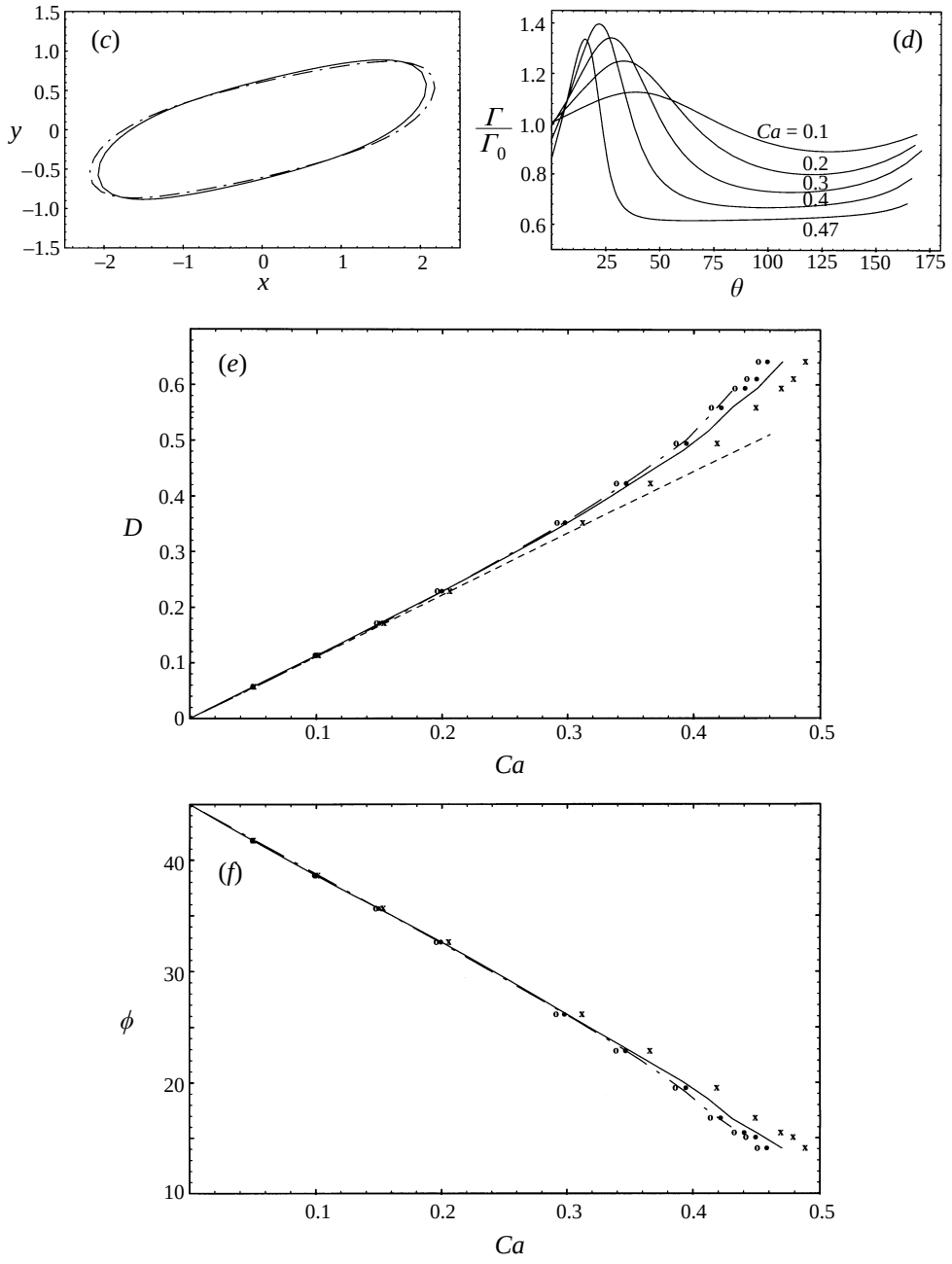

FIGURE 4. Results for a $Pe = O(1)$ case with $\chi = 0, \alpha = 10, \beta = 0.1$. (*a*) The steady drop shape at $Ca = 0.47$. (*b*) Same as (*a*), but for the surfactant distribution $\Gamma(v^1, v^2)$. (*c*) Cross-sections of the steady drop shapes in the (x, y)-plane at $Ca = 0.43$: ——, drops with non-uniform surface tension; —·—, constant-surface-tension drops. (*d*) The values of the surfactant concentration in the (x, y)-plane for $Ca = 0.1, 0.2, 0.3, 0.4$ and 0.47 as function of the meridional angle θ. (*e*) The deformation parameter D as a function of Ca: ——, drops with non-uniform surface tension. The filled circles, open circles, and x's show, respectively, the results with the effective capillary number defined with respect to the average, maximum, and minimum surface tension; – – –, from the small-deformation theory (2.7); —·—, for constant surface tension drops. (*f*) Same as (*e*), but for the inclination angle ϕ.

plotting the deformation parameter D and inclination angle ϕ against the capillary number, we obtain a generally good agreement with the corresponding results for a constant-surface-tension drop, as shown in figure 4 (*e,f*). Significant differences are observed only near the critical capillary number for continuous elongation, for $Ca > 0.35$. It is evident in figure 4 (*c*) for $Ca = 0.43$, that the deformation D is smaller than that for a constant-surface-tension drop, and the inclination angle ϕ is larger.

To explain these differences, in figure 4 (*d*) we present profiles of the surfactant concentration in the (x, y)-plane for several values of the capillary number. When Ca vanishes, the distribution is flat. As Ca is raised, the peak of the distribution at the tips tends to become sharper, while the profile becomes flatter at the waist, and the difference between the maximum and minimum value of the concentration becomes comparable to the mean. The accumulation of surfactants at the tips causes the surface tension to decrease and promotes the elongation. In contrast, the depletion of surfactant from the main body of the drop causes an increase in the surface tension, and restrains the continuous elongation. For example, when $Ca = 0.47$, the dimensionless surface tension $\gamma/(\mu ka)$ is larger than the initial value of 2.128 over more than half the interface.

Next, we consider replotting the results of figure 4 (*e,f*) in terms of a corrected capillary number that is defined with respect to an effective surface tension, with the objective of reducing the results for drops with surfactant to those for constant-surface-tension drops. To this end, we have several choices: we can define the corrected capillary number in terms of the mean value of the surface tension, as we have done previously for the low-Péclet-number case; we can use the nearly uniform value of the surface tension over the main body of the drop; or we can use the minimum value of the surface tension at the tips. We find that the second choice makes for the best agreement, as shown in figure 4 (*e,f*). Note, however, that the critical corrected capillary number in the presence of surfactants is still higher than that for a constant-surface-tension drop. Although useful in engineering computation, the simplified description cannot capture the delicate features of this complex flow.

Stone & Leal (1990) studied the corresponding deformation of drops in axisymmetric elongational flow. For values of α and β identical to those used in this case study, the deformation and inclination curves of Ca for a drop with surfactants almost overlapped with those for a constant-surface-tension drop, and the critical capillary numbers were virtually identical. This behaviour is in partial contrast with that emerging from our studies of simple shear flow. The differences must be attributed to the effect of the vorticity of the incident flow, which is exacerbated by the presence of the surfactant. The effect of the vorticity will be discussed further in § 5.

4.3. *Large Péclet number*

The third set of values of the dimensionless parameters, $\chi = 0.6, \alpha = 1000$ and $\beta = 0.3$, is chosen with the purpose of illustrating the behaviour of the drop when the magnitude of the Péclet number is large, in this case, $Pe = O(100)$. The streamlines of the unperturbed flow are shown in figure 1 (*c*). The incident flow convects the surfactant towards the tips of the elongating drop, but diffusive transport becomes significant when the concentration gradients have become sufficently large. The accumulation of the surfactant at the tips causes a local decrease in surface tension especially at high capillary numbers, as shown in figure 5 (*a–c*). We shall see in § 5 that the tangential component of the velocity along the interface illustrated in figure 5 (*a*) points in the same direction around the whole of the contour of the drop.

Figure 5 (*a*) reveals that the gradients of the surface tension are large at the tips but small over the main body of an elongated drop. The implied discontinuity in the tangential component of the jump in the interfacial traction can be regarded as the counterpart of the Marangoni stress exerted on a free surface. The tangential force field near the tips retards the motion of the fluid and thus reduces the magnitude of the interfacial velocity. Effectively, the drop behaves as though it were occupied by a more viscous fluid. This remark is consistent with the results shown in figure 5 (*d, e*) regarding the drop deformation and orientation.

The deformation of a drop with surfactants was found to be higher than that of a constant-surface-tension drop, and the inclination was found to be consistently smaller, even though the surface tension is elevated over the main body of the drop owing to depletion of the surfactant. In a comprehensive experimental investigation, Bentley & Leal (1986) showed that, when $\chi = 0.6$, maintaining the capillary number constant while increasing the viscosity ratio λ from the value of unity, promotes the drop deformation, causing it to align closer with the dividing streamline of the unperturbed flow.

The large variations in the surface tension make it difficult to define a corrected capillary number that would reconcile the deformation and inclination curves for drops with surfactants and constant-surface-tension drops. This difficulty is compounded by the observation that the shapes of the solid and dot-dashed lines in figure 5 (*d, e*) have significant differences in shapes. Surprisingly, the threshold value of the corrected capillary number above which a drop with surfactants continues to elongate, where the corrected capillary number is defined with respect to the average value of the surface tension, is nearly the same as that for a constant-surface-tension drop, which is placed at about 0.160.

Stone & Leal (1990) found that, when $\alpha = 1000$ and $\beta = 0.3$, the threshold value of the capillary number above which a drop with surfactants subjected to a uniaxial straining flow continues to elongate is smaller than that for a constant-surface-tension drop. We observe the converse behaviour. This difference serves to underline, once more, the importance of the type of the incident flow, especially at large values of the Péclet number where the coupling between the fluid mechanics and the scalar transport is strong.

4.4. *Effect of elasticity parameter* β

We have discussed the deformation of a drop under three sets of conditions corresponding to small, moderate, and large Péclet numbers, and for three types of incident flows. Next, we keep the property number α constant, and examine the effect of the elasticity parameter β expressing the sensitivity of the surface tension to the surfactant concentration, for a certain type of incident flow.

Typical results regarding the drop deformation, orientation, and distribution of surfactant for $\chi = 0.6, \alpha = 10$ and $\beta = 0.1, 0.5, 0.8$, are shown in figure 6. Figure 6 (*a, b*) illustrates the effect of the capillary number for each value of β. The Péclet number is on the order of unity, ranging from 0.4 to 2.6. Figure 6 (*c, d*) shows the surfactant distribution and drop contour in the (x, y)-plane for the most deformed stationary shapes.

Figure 6 (*a, b, d*) reveals that, when $\beta = 0.1$, the deformation and orientation curves, as well as the stationary drop shapes – all drawn with the solid lines – are virtually indistinguishable from those for a constant-surface-tension drop – drawn with dash-dotted lines. In this case, although the fluctuations in the surfactant concentration are substantial, the surface tension is nearly uniform over the whole of the interface. As β is increased, the surface tension becomes more sensitive to the surfactant

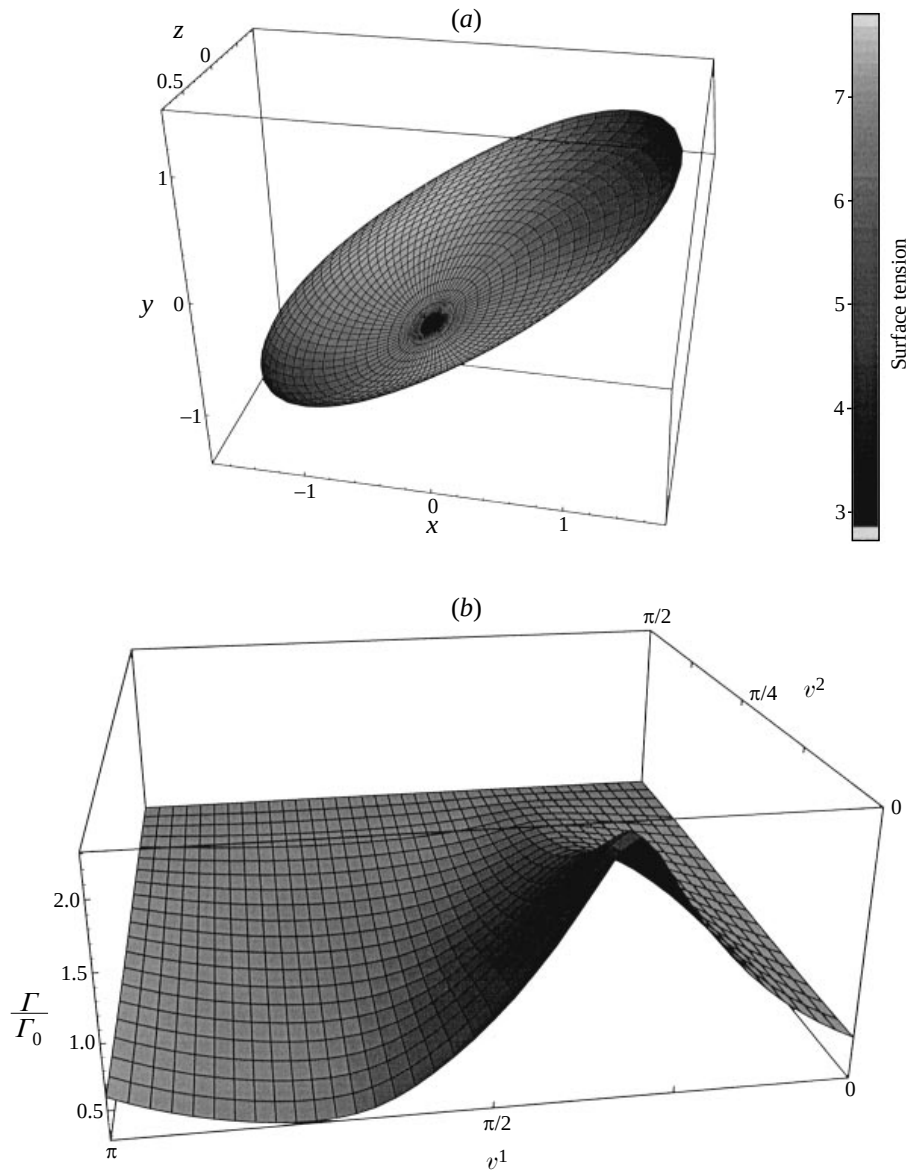

FIGURE 5(*a*, *b*). For caption see facing page.

concentration, and this results in larger tip deformations. But there is a secondary physical mechanism counteracting the deformation. The pronounced gradients of the surface tension inhibit the convective surfactant transport toward the tips, and thus reduce the surfactant concentration gradients, as shown in figure 6(*c*). The effect is not strong enough to halt the deforming action of the reduced surface tension due to surfactant redistribution. In the theoretical limit where β is unity, we expect a nearly uniform surfactant distribution, and a pronounced deformation with respect to that of a constant-surface-tension drop. But the physical relevance of this limit is undermined by the assumed linear relation between surface tension and surfactant concentration, as discussed in § 2.1.

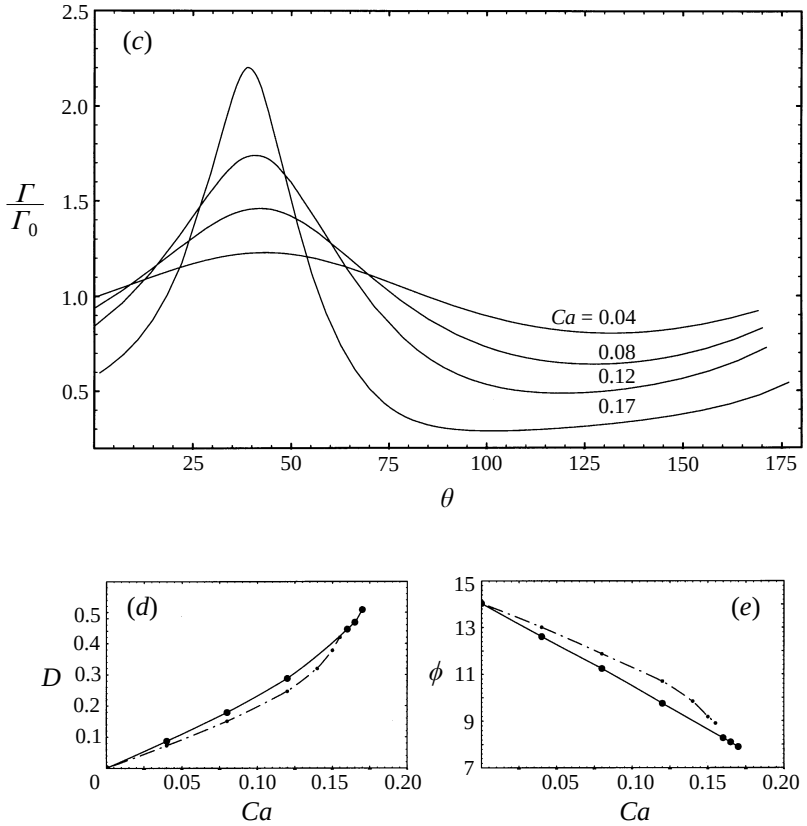

FIGURE 5. Results for a large-*Pe* case with $\chi = 0.6, \alpha = 1000, \beta = 0.3$. (*a*) The steady drop shape at $Ca = 0.17$. (*b*) Same as (*a*), but for the surfactant distribution $\Gamma(v^1, v^2)$. (*c*) The values of the surfactant concentration in the (x, y)-plane for $Ca = 0.04, 0.08, 0.12$, and 0.17 are plotted as function of the meridional angle θ. (*d*) The deformation parameter D as function of Ca: ——, drops with non-uniform surface tension; —·—, constant-surface-tension drops. (*e*) Same as (*d*), but for the inclination angle ϕ.

The increased interfacial area causes the surfactant to undergo a general dilution. For example, when $\beta = 0.8$, the surfactant concentration is nearly uniform over almost the whole of the interface, even near the critical capillary number for continuous elongation. Rescaling the capillary number using the average value of surface tension, we obtain good agreement with the results for constant-surface-tension drops. For the steady shapes shown in figure 6(*d*), the values of $\overline{Ca}$ are respectively equal to $0.153, 0.152$ and 0.157 for $\beta = 0.1, 0.5$ and 0.8, which is close to the critical value of the capillary number of a constant-surface-tension drop, 0.16.

Figure 6(*a*) shows that, at $\beta = 0.8$, the deformation and inclination of a drop is predicted accurately by the linear theory, represented by the dashed line, for an extended range of small and moderate capillary numbers up to the critical capillary number. At higher values of β, we obtain steady shapes with larger deformations, as shown in figure 6(*d*). This behaviour is in qualitative agreement with that reported by Stone & Leal (1990) for the analogous case of axisymmetric flow.

The trends remain unchanged when the conditions are changed so that the Péclet number becomes large. In figure 6(*e–h*) we present results for $\chi = 0.6, \alpha = 1000$, where

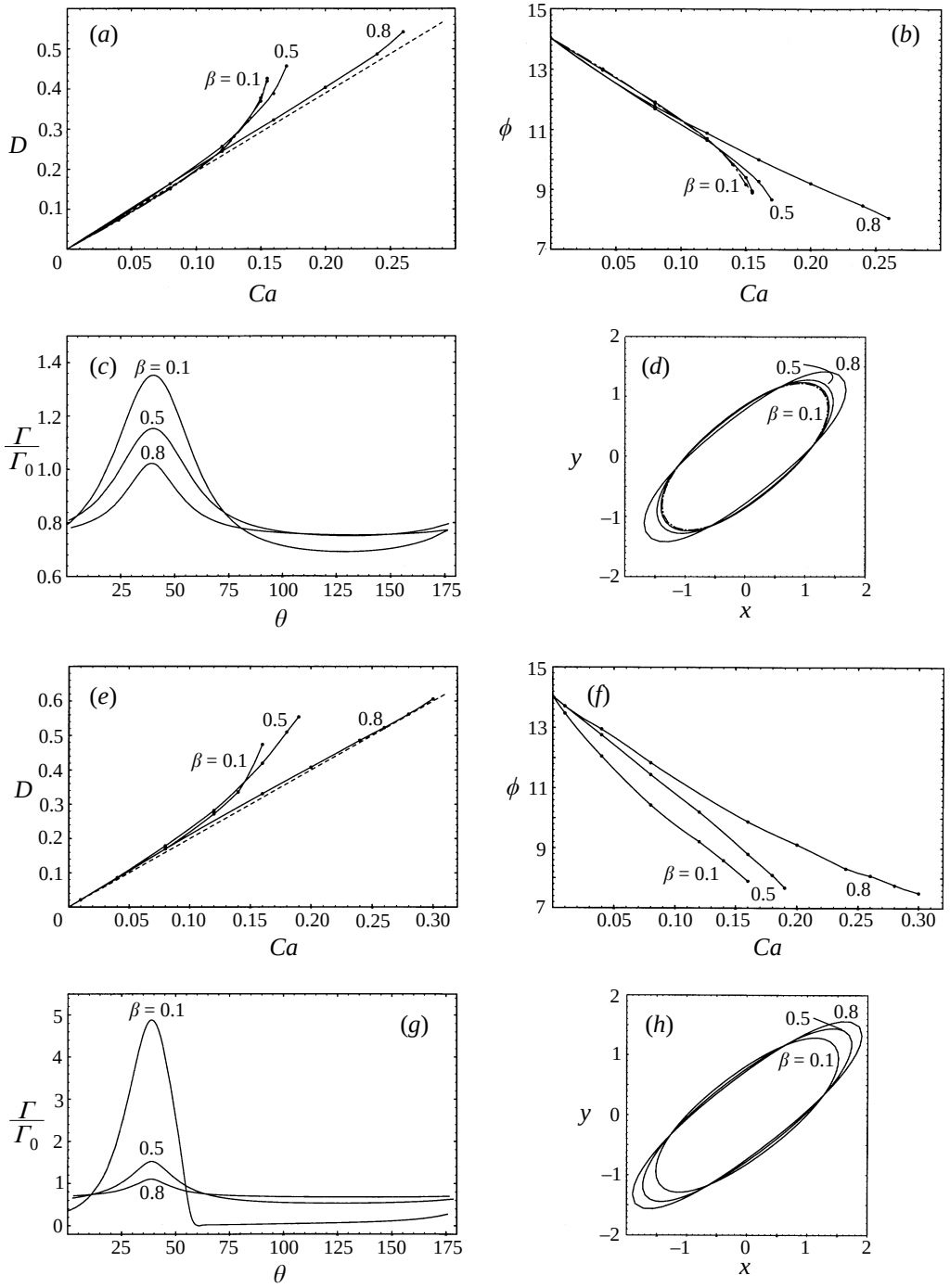

FIGURE 6. Effect of the elasticity parameter β. (a) The deformation parameter D as a function of Ca for $\chi = 0.6, \alpha = 10$: ——, drops with non-uniform surface tension; – – –, from the small-deformation theory; — - —, constant-surface-tension drops. (b) Same as (a) but for the inclination angle ϕ. (c) The cross-sections of the surfactant concentration distribution in the (x, y)-plane for the steady states of largest deformation. (d) Same as (c), but for steady drop shapes; the dash-dotted line shows the result for a constant-surface-tension drop. Same as (e–h) but for $\chi = 0.6, \alpha = 1000$.

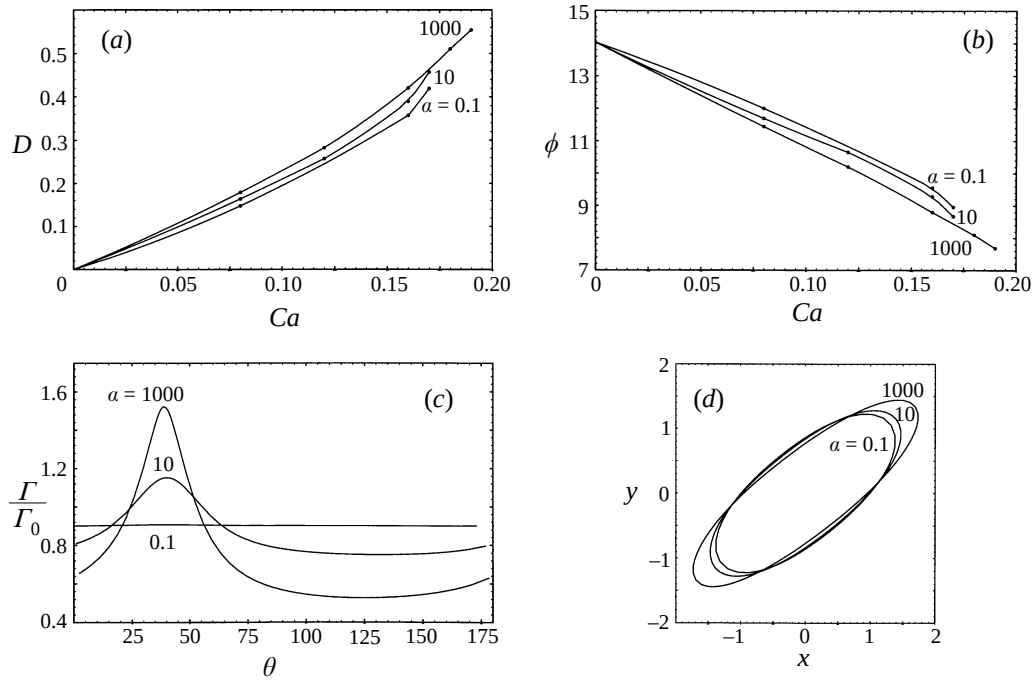

FIGURE 7. Effect of property number α. (a) The deformation parameter D as function of Ca for $\chi = 0.6, \beta = 0.5$ and $\alpha = 0.1, 10, 1000$. (b) Same as (a), but for the inclination angle ϕ. (c) The cross-sections of the surfactant concentration distribution in the (x, y)-plane for the steady states of largest deformation. (d) Same as (c), but for steady drop shapes.

the Péclet number ranges between 40 and 300. The strong effect of the convective surfactant transport is particularly evident in figure 6 (g) for $\beta = 0.1$. The main body of the drop is almost completely depleted of surfactants, while the concentration at the tips is nearly five times the initial value. Inspection of figure 6 (g) shows that as β is increased, the effective Péclet number is reduced, the surfactant distribution becomes increasingly more uniform, the average surface concentration diminishes, and the critical capillary number becomes notably larger. But the critical value of the corrected capillary number, defined with respect to the average surface tension, is nearly constant. For the most deformed shapes shown in figure 6 (h), the corrected critical values are equal to $0.158, 0.162$ or 0.164, for $\beta = 0.1, 0.5$ or 0.8.

4.5. *Effect of property number* α

In the second series of parametric investigations, we keep the elasticity parameter β fixed, and examine the effect of the property number α. Here, we want to study the effect of the surfactant diffusivity keeping all other physical parameters constant. This numerical investigation is the counterpart of physical experimentation where a drop that is covered with different types of surfactants with comparable elasticities but different diffusivities is introduced into a certain type of flow.

In figure 7, we present results for $\chi = 0.6, \beta = 0.5$ and three values of the property number $\alpha = 0.1, 10, 1000$. Similar results were obtained for other values of β. As α is increased, the convective motion causes the surfactant to accumulate, and lowers the surface tension at the tips, resulting in higher deformations. This behaviour is already

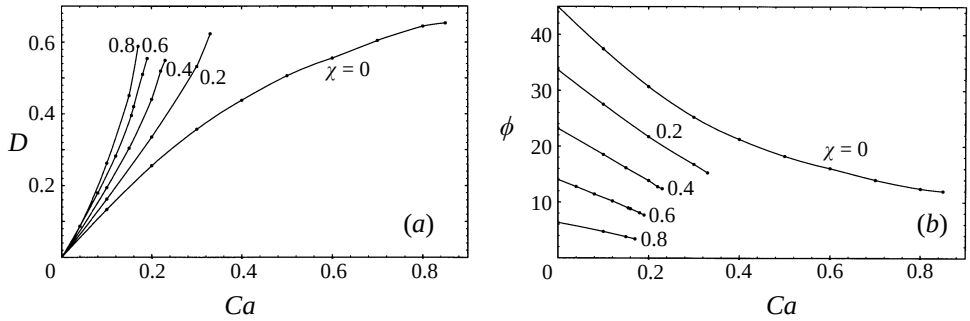

FIGURE 8. Effect of the flow type. (a) The deformation parameter D as function of Ca for $\alpha = 1000, \beta = 0.5$ and $\chi = 0, 0.2, 0.4, 0.6, 0.8$. ($b$) Same as ($a$), but for the inclination angle ϕ.

familiar from our discussion of the three case studies presented at the beginning of this section, and will not be elaborated. At a certain value of the capillary number, the deformation parameter increases, while the inclination angle decreases with increasing α, as shown in figure 7 (a, b). The critical capillary number for continued elongation is a monotonically increasing function of α. We note that this contrasts with the corresponding behaviour in uniaxial extensional flow studied by Stone & Leal (1990), which underlines once more the important effect of the vorticity of the incident flow.

4.6. *Effect of the structure of the incident flow*

When either the Péclet number Pe or the elasticity parameter β is small, the effect of the structure of the incident flow is similar to that for a clean drop at low values of the viscosity ratio $\lambda \leqslant 1$, as documented by Bentley & Leal (1986). We find, in particular, that for a fixed value of Ca, the deformation becomes more pronounced as χ is increased from the value of zero to the value of unity, and the incident flow changes from a simple shear flow to a purely straining two-dimensional flow. For all types of flow, the rate of change $\mathrm{d}D/\mathrm{d}Ca$ increases monotonically as Ca is raised, until the critical condition is reached where the drop can no longer sustain a stationary shape and continues to elongate. This behaviour is not surprising: the deforming action of a flow is made stronger as the magnitude of the rate-of-strain tensor overtakes that of the vorticity tensor.

When both Pe and β are sufficiently large, the effect of the structure of the incident flow becomes much more dramatic. In particular, as χ decreases from 0.8 to 0, the critical capillary number Ca_{cr} for continuous elongation increases from 0.18 to infinity, and the shape of the graph of the deformation versus capillary number undergoes notable qualitative changes. This behaviour is illustrated in figure 8 (a) where we present results for $\chi = 0.8, 0.6, 0.4, 0.2, 0$ and $\alpha = 1000, \beta = 0.5$. There is a corresponding strong effect on the inclination of the drop, as shown in figure 8 (b). Figure 8 (a) shows that $\mathrm{d}D/\mathrm{d}Ca$ for $\chi = 0$ (simple shear flow) is a monotonically decreasing function of Ca, and that D approaches a finite asymptotic value as Ca is raised. This behaviour is similar to that of clean drops at the high viscosity ratio $\lambda > 3.6$ and $\chi = 0$ (Kennedy *et al.* 1994). This analogy supports our earlier statement that surface tension gradients make the drops behave as if it were occupied by a higher-viscosity fluid.

5. Flow kinematics

In the preceding sections, we demonstrated that the vorticity of the incident flow and the interfacial stresses due to surfactant gradients play an important role in determining the magnitude of drop deformation and the critical capillary number for continuous elongation. To illustrate these effects in a more explicit manner, we now examine the structure of the flow around and inside stationary deformed drops.

When a drop is only slightly deformed and the surfactant distribution is nearly uniform, the internal and external velocity fields for viscosity ratio equal to unity, respectively denoted by $(\hat{u}, \hat{v})$ and (u, v), are given by (Stone & Leal 1990)

$$\begin{cases} \hat{u}(\boldsymbol{x}) = a_0(a_1 + x^2 + 5y^2)y, \\ \hat{v}(\boldsymbol{x}) = a_0(a_2 + x^2 + 5y^2)x, \end{cases} \quad \begin{cases} u(\boldsymbol{x}) = y + [b_1(1 - 5x^2/r^2) + b_2x^2]y/r^5, \\ v(\boldsymbol{x}) = \chi x + [b_1(1 - 5y^2/r^2) + b_2y^2]x/r^5, \end{cases} \tag{5.1}$$

where

$$a_0 = \frac{5}{4}\frac{1+\chi}{10+\epsilon}, \quad a_1 = -3 + \tfrac{2}{5}\zeta, \quad a_2 = -3 - \tfrac{2}{5}\zeta,$$

$$b_1 = (1+\chi)\left(-\frac{1}{2} + \frac{5}{2}\frac{1}{10+\epsilon}\right), \quad b_2 = (1+\chi)\left(-\frac{5}{2} + \frac{15}{2}\frac{1}{10+\epsilon}\right);$$

δ and ϵ were defined in § 2, and $\zeta = \delta(10 + \epsilon)$. Lengths have been normalized by the undeformed drop radius a, and velocities have been normalized by ka. We recall that δ expresses the relative magnitudes of the vorticity and the rate of strain of the incident flow, and ϵ expresses the importance of inhomogeneities in surface tension. It is evident then that the number of stagnation points in the interior and on the boundary of the drop, denoted by m, will depend on the value of the parameter ζ.

When $\zeta < 5$, $m = 9$, as shown in figure 9 (*a*): one stagnation point occurs at the drop centre; two stagnation points occur on the y-axis at the symmetric positions $(0, \pm[15-2\zeta]^{1/2})$; two stagnation points occur on the x-axis at the symmetric positions $(\pm\frac{1}{5}[15+2\zeta]^{1/2}, 0)$; and four stagnation points occur along the unit circle at $(\pm[\frac{1}{2}+\frac{1}{10}\zeta]^{1/2}, \pm[\frac{1}{2}-\frac{1}{10}\zeta]^{1/2})$. When $5 < \zeta < 15/2$, $m = 3$, as shown in figure 9 (*c*): the stagnation points on the y-axis and at the drop centre remain, but the others have disappeared. When $\zeta > 15/2$, $m = 1$, as shown in figure 9 (*e*): the only stagnation point is the drop centre.

As the flow changes from a planar extensional flow to simple shear flow, the number of stagnation points inside a clean drop, corresponding to $\epsilon = 0$, decreases from nine, to three, to one. Similar changes occur when we keep the value of δ constant and increase the magnitude of ϵ. Thus, the small-deformation theory reveals that the effect of inhomogeneities in surface tension is similar to that of the vorticity of the incident flow. This behaviour is consistent with our numerical results discussed in § 4 where we observed that for a fixed value of δ, the critical capillary number is a monotonically increasing function of ϵ, and for a fixed value of ϵ, the critical capillary number is a monotonically increasing function of δ.

In figure 9 (*a, c, e*), we present the streamline patterns in the (x, y)-plane for a fixed value of δ and different values of ϵ, computed from (5.1). Figure 9 (*a*) shows the streamline pattern for $\chi = 0.6, \alpha = 10, \beta = 0.1$, corresponding to $\zeta = \frac{25}{9}$. We observe a pair of large eddies rotating in the clockwise sense and centred at the y-axis, and a pair of smaller eddies rotating in the counter-clockwise sense and centred at the x-axis. Figure 9 (*c*) shows the streamline pattern for $\chi = 0.6, \alpha = 10, \beta = 0.5$, corresponding to $\zeta = 5$; the pair of smaller recirculating eddies have disappeared. The four stagnation points on the unit circle and the two stagnation points on the x-axis have been united

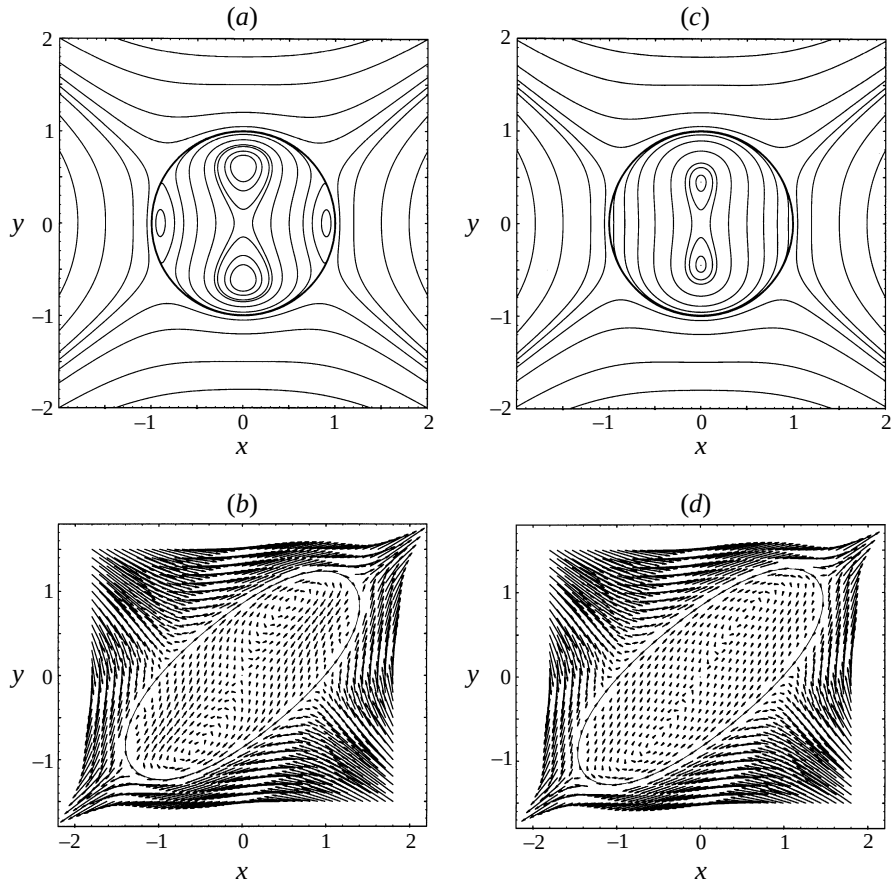

FIGURE 9(*a–d*). For caption see facing page.

into two stagnation points located at $(\pm 1, 0)$. Figure 9 (*e*) shows the streamline pattern for $\chi = 0.6, \alpha = 1000, \beta = 0.3$ corresponding to $\zeta = 109.6$. The two stagnation points on the drop surface have disappeared, and the two stagnation points on the y-axis have collapsed to the drop centre. The fluid within the drop rotates almost like a rigid body.

To illustrate the effect of drop deformation, in figure 9 (*b, d, f*) we present the velocity vector fields obtained from the results of our computations for highly deformed drops. Inspecting these patterns, and others drawn but not shown, we find that the number of recirculating eddies and the number of stagnation points over the interface are the same as those predicted by the small-deformation theory, at all capillary numbers up to the critical value for continuous elongation. This is in spite of the large drop deformation. Kennedy *et al.* (1994) found that the structure of the flow inside and around a clean drop is also insensitive to Ca for a wide range of viscosity ratios, $0.08 < \lambda < 6.4$. Drop deformation does not have a profound effect on the kinematics.

6. Effective rheological properties of dilute suspensions

Knowledge of the transient or stationary shape of a deformed drop, and of the instantaneous or asymptotic distribution of the surfactant over the interface, allows us to compute the effective stresses developing in a dilute suspension, using a well-

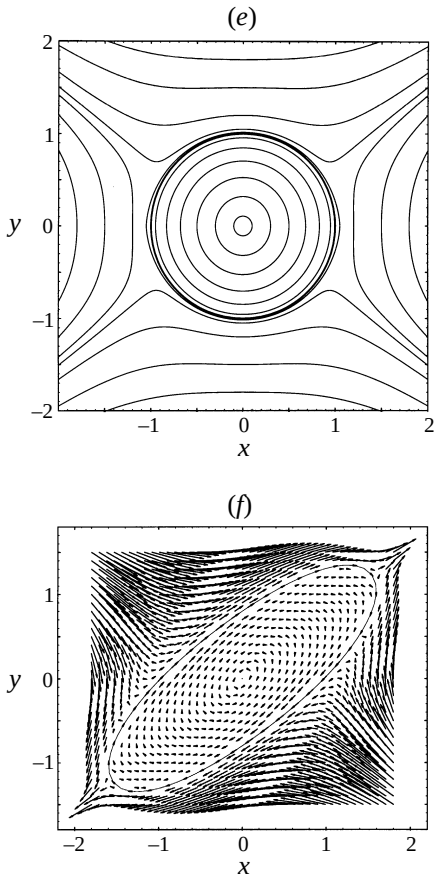

FIGURE 9. Flow field in the (x, y)-plane for $\chi = 0.6$ at different Péclet numbers. (*a*) The streamlines predicted by the small-deformation analysis for $\alpha = 10$ and $\beta = 0.1$. (*b*) The flow field and drop shape for $\alpha = 10, \beta = 0.1$ at $Ca = 0.155$. (*c*) Same as (*a*), but for $\beta = 0.5$. (*d*) Same as (*b*), but for $\beta = 0.5$ at $Ca = 0.17$. (*e*) Same as (*a*), but for $\alpha = 1000$ and $\beta = 0.3$. (*f*) Same as (*b*), but for $\alpha = 1000, \beta = 0.3$ at $Ca = 0.17$.

established formalism of continuum mechanics (Batchelor 1970). When the viscosity ratio is equal to unity, knowledge of the flow field around and inside the drop is not required (Pozrikidis 1993).

In this section, we discuss the effect of the surfactant on the effective rheological properties of a dilute suspension in simple shear flow corresponding to $\chi = 0$. Previous studies have shown that a dilute suspension of clean drops behaves like a shear-thinning medium with some elastic behaviour similar to that exhibited by polymeric solutions (e.g. Kennedy *et al.* 1994).

The effective stress tensor $\langle \boldsymbol{\sigma} \rangle$ of a suspension of drops with viscosity ratio equal to unity is given by (Pozrikidis 1995)

$$\langle \sigma_{ij} \rangle = -\delta_{ij} \langle P \rangle + 2\mu \langle e_{ij} \rangle + \mathrm{c} \frac{3}{4\pi \mathrm{a}^3} \int_{S_D} \Delta f_i x_j \, \mathrm{d}S, \tag{6.1}$$

where $\langle\ \rangle$ denotes volume average values, and c is the volume fraction of the drops in the suspension. The integral on the right-hand side of (6.1) multiplied by $3/(4\pi \mathrm{a}^3)$ is the *particle stress tensor*, which will be denoted by Σ_{ij}. The discontinuity in the

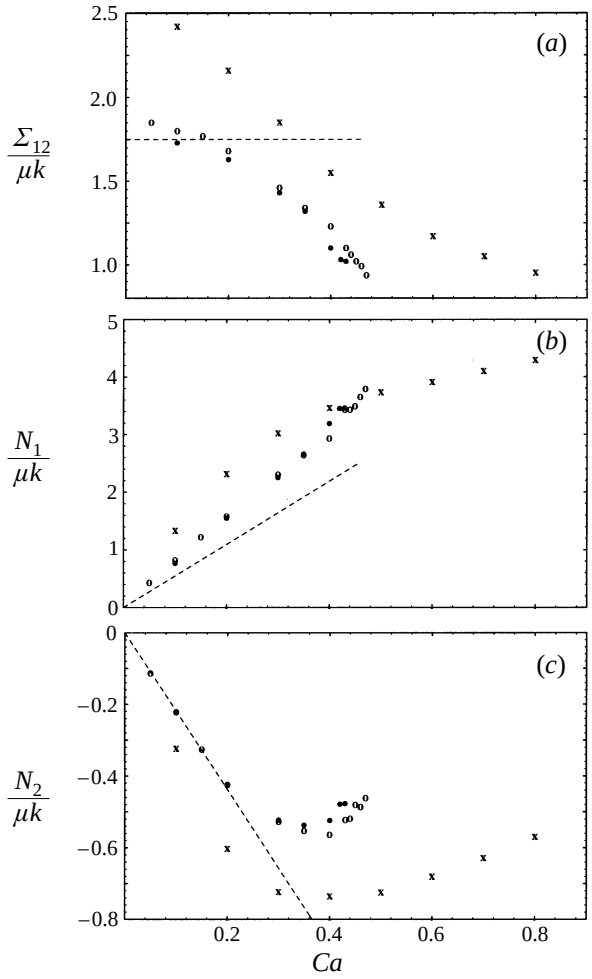

FIGURE 10. (*a*) The shear component of the particle stress tensor $\Sigma_{12}/(\mu k)$ for simple shear flow ($\chi = 0$) as a function of Ca: •, constant surface tension ($\beta = 0$); – – –, prediction of the small-deformation result of Schowalter *et al.* (1968) for constant surface tension; **o**, $\alpha = 10, \beta = 0.1$; **x**, $\alpha = 1000, \beta = 0.5$. (*b*) Same as (*a*), but for the first normal stress $N_1/(\mu k)$. (*c*) Same as (*a*), but for the second normal stress $N_2/(\mu k)$.

interfacial traction is given in equations (2.4) and (2.5) in terms of the surfactant concentration.

In figure 10, we plot the shearing component of the particle stress tensor Σ_{12} and first and second normal stress differences $N_1 = \Sigma_{11} - \Sigma_{22}, N_2 = \Sigma_{22} - \Sigma_{33}$, against the capillary number Ca, for stationary deformed drops, up to the critical capillary number for continuous elongation. The three sets of data indicated with solid circles, hollow circles, and x's, correspond, respectively, to a dilute suspension of constant-surface-tension drops with $\beta = 0$, a suspension of drops with weak Marangoni stresses, with $\alpha = 10, \beta = 0.1$, and a suspension with strong Marangoni stresses with $\alpha = 1000, \beta = 0.5$. The dashed line represents the predictions of the small-deformation theory of Schowalter, Chaffey & Brenner (1968) for drops with constant surface tension. The asymptotic predictions for Σ_{12} and N_2 agree well

with the numerical results at small and moderate deformations, but significantly underestimate the value of N_1 when the capillary number is not exceedingly small.

The three sets of symbols show similar features in a qualitative sense, but with significant quantitative differences. It is important to note that these differences are much more pronounced than those regarding the drop deformation and inclination discussed in the preceding sections. The effect of the surfactant is stronger on the rheology of a suspension than on the actual shape of the deformed drops.

In all cases, as Ca is raised, the reduced shear stress $\Sigma_{12}/(\mu k)$ and the first normal stress difference $N_1/(\mu k)$ increase monotonically, while the negative of the second normal stress difference $N_2/(\mu k)$ increases, reaches a maximum, and then starts to decline. The behaviour exhibited in these graphs is typical of a medium with a shear-thinning and some elastic behaviour. As variations in surface tension become more significant, the drops behave as if they were occupied by a higher-viscosity fluid. Accordingly, as the Marangoni stresses become larger while the drop deformation and thus Ca remain small, the fluid inside the drop tends to rotate like a rigid body, and $\Sigma_{12}/(\mu k)$ approaches the limit 2.5, corresponding to a dilute suspension of rigid particles with spherical shapes.

7. Concluding remarks

We have studied the effect of an insoluble surfactant on the deformation and on the structure of the flow inside and around a deformable drop immersed in a linear ambient flow. Our computations are restricted to the case where the viscosity of the drop is equal to that of the ambient fluid. The results showed that, in this case, the surfactant has a significant but not radical effect on the magnitude of the drop deformation and inclination. Convection of surfactant towards the tips of the deformed drop exacerbates the local deformation by lowering the surface tension; dilution of surfactant due to the increased interfacial area and elevated surface tension over the main body of the drop restrains the deformation. In most cases, the critical capillary number for continuous elongation can be predicted from that of a clean drop, provided that a correction is made to account for the effect of surfactant dilution. Surprisingly, good estimates are obtained even when the surfactant distribution is notably inhomogeneous, and the surface tension shows significant variations.

The vorticity of the incident flow plays an important role in determining the effect of the surfactant. The associated rotational motion may either increase or decrease the critical capillary number for continuous elongation. The effect of the vorticity is enhanced when the interfacial tension gradients are large and the drop behaves as if it were occupied by a more viscous fluid.

Extensions of the present studies can be made into several directions. One extension concerns the effect of the viscosity ratio; a second concerns the effect of surfactant solubility; and a third concerns the effect of surfactant saturation. Leal and coworkers and Pawar & Stebe (1996) studied all of these effects for axisymmetric deformation in uniaxial straining flow. Milliken & Leal (1994), in particular, confirmed that the mass transport with the bulk of the fluid reduces the interfacial surfactant concentration and surface tension gradients. Similar effects are expected for three-dimensional flow. Pawar & Stebe (1996) find that the choice of the interfacial constitutive equation has a profound effect on the magnitude of drop deformation, distribution of the surfactant, and evidently on the structure of the velocity field and on the rheology of dilute suspensions. In particular, surface saturation suppresses tip stretching leading

to smaller deformations. At the present time, high computational cost prevents us conducting a comprehensive and systematic investigation.

Another important extension can be made in the direction of examining the effect of a surfactant on the rheology and collective motion of drops in a non-dilute suspension. Pozrikidis (1993) studied the motion of an ordered suspension, and Loewenberg & Hinch (1996) considered the motion of a random suspension, both in the absence of surfactants, in a simple shear flow. But high computational cost is a hindrance, and even a compromise in accuracy is prevented by considerations of numerical stability in solving the convection–diffusion equation.

Appendix. Intrinsic equations of surface motion

Let Ω be a section of a deforming material surface in the three-dimensional space, and Γ be the concentration of a scalar transported quantity that is defined over the surface.

The rate of change of the total amount of the scalar quantity residing in Ω is given by

$$\frac{\mathrm{d}}{\mathrm{d}t}\int_{\Omega}\Gamma\,\mathrm{d}S = -\int_{\partial\Omega}\boldsymbol{q}\cdot\boldsymbol{b}\,\mathrm{d}l, \tag{A 1}$$

where $\boldsymbol{q}$ denotes the surface flux across the surface boundary $\partial\Omega$, $\boldsymbol{b}$ is the binormal vector to the curve $\partial\Omega$, and l is the arclength measured along $\partial\Omega$. To express this conservation law in differential form, we introduce a curvilinear coordinate system consisting of two Lagrangian variables ξ and η on the surface. The left-hand side of (A 1) can be rewritten as

$$\frac{\mathrm{d}}{\mathrm{d}t}\int_{\Omega}\Gamma h_S\,\mathrm{d}\xi\mathrm{d}\eta = \int_{\Omega}\left(\frac{\mathrm{D}\Gamma}{\mathrm{D}t}h_S + \Gamma\frac{\mathrm{D}h_S}{\mathrm{D}t}\right)\mathrm{d}\xi\mathrm{d}\eta = \int_{\Omega}\left(\frac{\mathrm{D}\Gamma}{\mathrm{D}t} + \Gamma\frac{1}{h_S}\frac{\mathrm{D}h_S}{\mathrm{D}t}\right)\mathrm{d}S, \tag{A 2}$$

where h_S is the interfacial areal metric coefficient, $\mathrm{d}S = h_S\,\mathrm{d}\xi\mathrm{d}\eta$, and $\mathrm{D}/\mathrm{D}t$ denotes the material derivative. Using the divergence theorem to modify the right-hand side of (A 1), and substituting the right-hand side of (A 2) into the left-hand side of (A 1), we obtain

$$\int_{\Omega}\left(\frac{\mathrm{D}\Gamma}{\mathrm{D}t} + \Gamma\frac{1}{h_S}\frac{\mathrm{D}h_S}{\mathrm{D}t}\right)\mathrm{d}S = -\int_{\Omega}\nabla_s\cdot\boldsymbol{q}\,\mathrm{d}S, \tag{A 3}$$

where ∇_s is the surface gradient operator, $\nabla_s = (\boldsymbol{I}-\boldsymbol{nn})\cdot\nabla$. Since (A 3) holds for an arbitrary Ω, we discard the integral operator and obtain the differential transport equation

$$\frac{\mathrm{D}\Gamma}{\mathrm{D}t} + \Gamma\frac{1}{h_S}\frac{\mathrm{D}h_S}{\mathrm{D}t} = -\nabla_s\cdot\boldsymbol{q}. \tag{A 4}$$

In practice, we use curvilinear surface coordinates (v^1, v^2) whose grid lines do *not* necessarily move with the velocity of the surface $\boldsymbol{u}$. Instead, the velocity of the coordinate lines is given by

$$\boldsymbol{v} = (\boldsymbol{u}\cdot\boldsymbol{n})\boldsymbol{n} + \boldsymbol{w}, \tag{A 5}$$

where $\boldsymbol{w}$ is an arbitrary vector tangential to the surface. If $\boldsymbol{w} = \boldsymbol{n}\times\boldsymbol{u}\times\boldsymbol{n}$, then $\boldsymbol{v} = \boldsymbol{u}$; if $\boldsymbol{w} = 0$, then $\boldsymbol{v} = (\boldsymbol{u}\cdot\boldsymbol{n})\boldsymbol{n}$.

The time rate of change of a material surface element can be written as (equation (1.4.25) in Pozrikidis 1996)

$$\frac{1}{h_S}\frac{\mathrm{D}h_S}{\mathrm{D}t} = \nabla_s\cdot\boldsymbol{u}. \tag{A 6}$$

Expressing the material derivative $\mathrm{D}\Gamma/\mathrm{D}t$ in the form

$$\left(\frac{\partial \Gamma}{\partial t}\right)_{v^1,v^2} + [\boldsymbol{n}\times\boldsymbol{u}\times\boldsymbol{n}-\boldsymbol{w}]\cdot\nabla\Gamma \tag{A 7}$$

and assuming that the surface flux is given by Fick's law

$$\boldsymbol{q} = -\mathscr{D}_s\nabla_s\Gamma, \tag{A 8}$$

we obtain an unsteady convection–diffusion equation for Γ, written in the arbitrary curvilinear coordinates (v^1, v^2):

$$\left(\frac{\partial \Gamma}{\partial t}\right)_{v^1,v^2} + [\boldsymbol{n}\times\boldsymbol{u}\times\boldsymbol{n}-\boldsymbol{w}]\cdot\nabla\Gamma + \Gamma\nabla_s\cdot\boldsymbol{u} - \mathscr{D}_s\nabla_s^2\Gamma = 0, \tag{A 9}$$

Expressions for $\nabla_s\cdot\boldsymbol{u}$ and $\nabla_s^2\Gamma$ in general curvilinear coordinates (v^1, v^2) are given by Stone & Leal (1990). An independent derivation of equation (A 9) in curvilinear coordinates was recently presented by Wong *et al.* (1996).

We thank Professor Ali Borhan for his useful comments on the manuscript. This project was supported by the National Science Foundation and the SUN Microsystems Corporation. Acknowledgment is made to the donors of the Petroleum Research Fund, administered by the American Chemical Society, for partial support of this research.

REFERENCES

Abramowitz, M. & Stegun, I. A. 1972 *Handbook of Mathematical Functions.* Dover.

Adamson, A. W. 1976 *Physical Chemistry of Surfaces*, 3rd edn. John Wiley & Sons.

Barthès-Biesel, D. & Rallison, J. M. 1981 The time-dependent deformation of a capsule freely suspended in a linear shear flow. *J. Fluid Mech.* **117**, 251–267.

Batchelor, G. K. 1970 The stress system in a suspension of force-free particles. *J. Fluid Mech.* **41**, 545–570.

Bentley, B. J. & Leal, L. G. 1986 An experimental investigation of drop deformation and breakup in steady two-dimensional linear flows. *J. Fluid Mech.* **167**, 241–283.

Borhan, A. & Mao, C.-F. 1992 Effect of surfactants on the motion of drops through circular tubes. *Phys. Fluids* A **4**, 2628–2640.

Boulton-Stone, J. M. 1995 The effect of surfactant on bursting gas bubbles. *J. Fluid Mech.* **302**, 231–257.

Bruijn, R. A. de 1989 Deformation and breakup of drops in simple shear flows. PhD thesis, Tech. Univ. Eindhoven.

Bruijn, R. A. de 1993 Tipstreaming of drops in simple shear flows. *Chem. Engng Sci.* **48**, 277–284.

Clift, R., Grace, J. R. & Weber, M. E. 1974 Stability of bubbles in fluidized beds. *Indust. Engng Chem. Fundam.* **13**, 45–51.

Defay, R. & Prigogine, I. 1966 *Surface Tension and Adsorption.* (with the collaboration of A. Bellemans. Translated by D. H. Everett). John Wiley & Sons.

Evans, E. A. & Skalak, R. 1980 *Mechanics and Thermodynamics of Biomembranes.* CRC Press.

Flumerfelt, R. W. 1980 Effects of dynamic interfacial properties on drop deformation and orientation in shear and extensional flow fields. *J. Colloid Interface Sci.* **76**, 330–349.

Gaver, D. P. & Grotberg, J. B. 1990 The dynamics of a localized surfactant on a thin film. *J. Fluid Mech.* **213**, 127–148.

Harper, J. F. 1982 Surface activity and bubble motion. *Appl. Sci. Res.* **38**, 343–352.

He, Z., Dagan, Z. & Maldarelli, C. 1991 The influence of surfactant adsorption on the motion of a fluid sphere in a tube. Part 1. Uniform retardation controlled by sorption kinetics. *J. Fluid Mech.* **222**, 1–32.

Ji, W. & Setterwall, F. 1994 On the instabilities of vertical falling liquid films in the presence of surface-active solute. *J. Fluid Mech.* **278**, 297–323.

Kennedy, M. R., Pozrikidis, C. & Skalak, R. 1994 Motion and deformation of liquid drops and the rheology of dilute emulsions in simple shear flow. *Computers Fluids* **23**, 251–278.

Levich, V. G. & Krylov, V. S. 1969 Surface-tension-driven flow phenomena. *Ann. Rev. Fluid Mech.* **1**, 293–316.

Li, X. & Pozrikidis, C. 1996 Shear flow over a liquid drop adhering to a solid surface. *J. Fluid Mech.* **307**, 167–190.

Loewenberg, M. & Hinch, E. J. 1996 Numerical simulation of a concentrated emulsion in shear flow. *J. Fluid Mech.* **321**, 395–419.

Lu, H. & Apfel, R. E. 1991 Shape oscillations of drops in the presence of surfactants. *J. Fluid Mech.* **222**, 351–368.

Mavrovouniotis, G. M. & Brenner, H. 1993 A micromechanical investigation of interfacial transport processes. I. Interfacial conservation equations. *Phil. Trans. R. Soc. Lond.* A **345**, 165–107.

Milliken, W. J. & Leal L. G. 1994 The influence of surfactant on the deformation and breakup of a viscous drop: The effect of surfactant solubility. *J. Colloid Interface Sci.* **166**, 275–285.

Milliken, W. J., Stone, H. A. & Leal L. G. 1993 The effect of surfactant on trasient motion of Newtonian drops. *Phys. Fluids* A **5**, 69–79.

Park, C., Maruvada, S. R. & Yoon, D. 1994 The influence of surfactant on the bubble motion in Hele-Shaw cells. *Phys. Fluids* A **6**, 3267–3275.

Pawar, Y. & Stebe, K. J. 1996 Marangoni effects on drop deformation in an extensional flow: The role of surfactant physical chemistry. I. Insoluable surfactants. *Phys. Fluids* A **8**, 1738–1751.

Pozrikidis, C. 1992 *Boundary Integral and Singularity Methods for Linearized Viscous Flow*. Cambridge University Press.

Pozrikidis, C. 1993 On the transient motion of ordered suspensions of liquid drops. *J. Fluid Mech.* **246**, 301–320.

Pozrikidis, C. 1995 Finite deformation of liquid capsules enclosed by elastic membranes in simple shear flow. *J. Fluid Mech.* **297**, 123–152.

Pozrikidis, C. 1996 *Introduction to Theoretical and Computational Fluid Dynamics*. Oxford University Press.

Rallison, J. M. 1984 The deformation of small viscous drops and bubbles in shear flows. *Ann. Rev. Fluid Mech.* **16**, 45–66.

Schowalter, W. R., Chaffey, C. E. & Brenner, H. 1968 Rheological behavior of a dilute emulsion. *J. Colloid Interface Sci.* **26**, 152–160.

Stone, H. 1994 Dynamics of drop deformation and breakup in viscous fluids. *Ann. Rev. Fluid Mech.* **26**, 65–102.

Stone, H. A. 1990 A simple derivation of the time-dependent convection-diffusion equation for surfactant transport along a deforming interface. *Phys. Fluids* A **2**, 111–112.

Stone, H. A. & Leal, L. G. 1990 The effects of surfactants on drop deformation and breakup. *J. Fluid Mech.* **222**, 161–186.

Tian, Y., Holt, R. G. & Apfel, R. E. 1995 Investigations of liquid surface rheology of surfactant solutions by droplet shape oscillations: theory. *Phys. Fluids* A **7**, 2938–2949.

Wong, H., Rumschitzki, D. & Maldarelli, C. 1996 On the surfactant mass balance at a deforming fluid interface. *Phys. Fluids* A **8**, 3203–3204.